**NTNU – Trondheim**
Norwegian University of
Science and Technology

# Doppler radar speed measurement on board

digital signal processing

Feng Feng

Master of Science in Electronics
Submission date: June 2013
Supervisor: Torbjørn Ekman, IET
Co-supervisor: Anders Hagen, QFree

Norwegian University of Science and Technology
Department of Electronics and Telecommunications

# Preface

This report is submitted in partial fulfillment of the requirements for the degree of Master of Science at the Norwegian University of Science and Technology (NTNU). The work is supported by Q-Free, which is a technology supplier of products for road pricing and road traffic control in Trondheim, Norway.

The topic develops in two directions: the software and the signal processing. Joacim Dybedal worked on the software, and I selected the signal processing. This thesis concentrates on the modeling of the radar system, discussing the different algorithms for the power spectrum density (PSD) estimation.

I selected this topic because I think it is an interesting subject. The radar speed measurement is a common factor in our lives, and I always wondering about how it works. In addition, I worked not only the theory part, but also on the practical measurements, and we shall output a real solution: both the software and the algorithm. Prior to the digital signal processing knowledge, I gained certain experience in using Matlab, which is an efficient assistant with signal processing.

I would like to thank Anders Hagen, who works at Q-Free and is my contact person there. My major is in design of digital systems, and I did not have much background in digital signal processing. I appreciate the fact that he trusted me and allowed me to do this thesis, so that I have had the chance to study digital signal processing.

I also have to extend my gratitude to my supervisor, Torbjørn Ekman, who is the associated Professor in channel modeling at NTNU. I met with him once a week and received many practical tips from him. It would have been hard for me to complete my master thesis without his help.

Moreover, I want to thank Joacim Dybedal, who worked with the software. We shared the data and had discussions about the subject. Finally, I want to thank Linda March, who helped me to check my English grammar in this thesis.

# Abstract

Doppler radars have been widely used in many different fields, such as traffic control, weather prediction, navigation, satellite tracking, Airborne Early Warning systems and missile guidance. The technology company Q-free in Trondheim intends to test the application of the Doppler radar module MDU 2410 in speed measurement. In this thesis a method was presented to measure the speed of a vehicle with this radar module.

The most frequently used method to analyze the Doppler signal is spectrum estimation. This thesis concentrates on the discussions about the different algorithms for PSD estimation. Both the classical spectrum estimation methods, such as the periodogram, the Bartlett method, the Welch method and the BT method, and the modern PSD estimation methods like ARMA process, AR process and MA process, were introduced.

The AR model is the most widely used among these three parametric models. There are two main reasons. Firstly, the AR model is suitable for representing spectra with narrow peaks. Secondly, the AR model results in very simple linear equations for the AR parameters. On the other hand, the MA model, as a general rule, requires many more coefficients to represent a narrow spectrum. Consequently, it is rarely used by itself as a model for spectrum estimation. By comparing the spectra of the AR model with the other spectra based on the classical spectrum estimations, the advantages of the AR model are obvious. The resolution is high; the ability of anti-interference is strong, and the peak value is clear. As a result it was determined that the AR should be implemented in this system.

The measured results reveal that the order value in the AR model affects the accuracy of calculation results. To reach a precise velocity, the order should be dynamic in the calculations. After a series tests, the order is determined to begin with 23, and then decreases gradually when the velocity of the vehicle reaches 20 km/h.

This thesis can be continued with further discussions on the AR model. There may be other methods for discovering the velocity with higher levels of accuracy.

# Abbreviations

ARMA – Autoregressive Moving Average
AR – Autoregressive
BT method – Blackman and Tukey method
DC – Direct Current
FFT – Fast Fourier Transform
IF – Intermediate Frequency
MA – Moving Average
PSD – Power Spectrum density
RF – Radio Frequency
SD card - SD (Secure Digital) Memory Card

# Contents

# List of figures

# List of tables

# 1. Introduction

## 1.1 General

The Doppler Effect was proposed by the Austrian physicist, Christian Doppler, in 1842. It states that the observed frequency is increasing when the wave source is moving towards the observer. Otherwise, the observed frequency reduces. It is a common phenomenon in all kinds of waves, such as sound waves, water waves, microwaves and so on, but the Doppler Effect is difficult to observe in the microwave without any instrumentation. The most commonly found Doppler Effect in our daily life is in the sound wave. For example, a motorbike is approaching from a distance, and you can hear the sound of the motor getting louder. When the motorbike has passed and is traveling away from you, you can hear the sound getting low again. This change in the sound frequency is due to the Doppler Effect.

Many kinds of measurement applications are based on the Doppler Effect. The Doppler radar speed measurement system is one typical example of the Doppler Effect application in sound waves. Other systems, such as the temperature measurement system, weather prediction system and some applications used in astronomy, are examples of the Doppler Effect in microwaves.

## 1.2 Motivation and objective

Today there are various popular methods for the measurement of speed, for example, by measuring the rotation speed of the vehicle's wheels to obtain the velocity of cars or trains. To measure the speed of a ship or aircraft, GPS or Doppler radar is competent. With the development of radar technology, the accuracy, reliability and real-time ability are improving. On the other hand, due to idle running and slipping, the methods of measuring the rotation speed of the wheel may be considered suitable for replacement. The GPS speed measurement can avoid these limitations caused by measuring the rotation speed of the wheels, but it may show errors when the vehicle is running in tunnels, because the GPS signal is blocked by the tunnel. In the Doppler radar speed measurement system, the radar transmits microwaves to the road surface and receives the reflected signal. By signal processing, the corresponding velocity of the vehicle can be worked out. This system is much more flexible, but it relies on the calculation accuracy, algorithm selection and the system components.

The company, Q-Free at Trondheim in Norway, is a supplier of technology products for road pricing and road traffic control. They want to carry out research on the application of Doppler radar in the speed measurement of vehicles. One 24-GHz Doppler radar should be mounted on a vehicle. The radar transmits microwaves and receives the reflected signal and then mixes the transmitted signal and the received signal. Output is the intermediate frequency (IF) signal. Signal processing technology is needed to process and analyze the IF signal and find out the peak value in the power spectrum density (PSD) with respect to the Doppler frequency. Once the Doppler

frequency is determined, the respond velocity of the vehicle can be confirmed by some computations.

## 1.3 Scope of the work

This scope of the work is listed below:

1. How to build a model to estimate the radar signal.
2. How to select a proper algorithm for this speed measurement system.
3. How to measure the real velocity of the vehicle.
4. How to analyze the received radar signal and get a spectrum.
5. How to find out the velocity from the spectrum.

## 1.4 Limitations

This thesis is based on the following assumptions:

1. This project employs the 24.1 GHz continuous wave Doppler radar; all the calculations and analysis are based on this Doppler radar module.
2. The radar cross section (RCS) referred to in other articles can be used in this system.
3. The road surface is perfectly dry.

## 1.5 Overview of the thesis

The thesis is organized as follows:

Chapter 1 introduces the background of the Doppler Effect, the motivation of the thesis, the thesis structure and its limitations.

Chapter 2 describes the theory of the Doppler Effect and the principle of the measurement system. It also presents some other applications of Doppler radar and describes some frequently used spectrum estimation methods.

Chapter 3 shows the modeling process with the help of Matlab. It presents how to use a geometric model to simulate the system. The PSD estimation is based on this model.

Chapter 4 shows the simulation results. The algorithms introduced for spectrum estimations in Chapter 2 are simulated here. Both the advantages and disadvantages are illustrated in the figures. As a result, the algorithm that should be implemented in the system is indicated.

Chapter 5 shows the practical measured data and compares the estimated results based on the model and the real measured data.

Chapter 6 summarizes the results from each stage. It also lists some drawbacks, which should be improved in the future.

# 2. Literature survey

This chapter states the background of this thesis. It introduces the theory behind how the Doppler radar works. It reveals the Doppler Effect and the equations to calculate the Doppler frequency. The principle of the speed measurement is described. Some other applications based on the Doppler Effect are also presented. Finally, it introduces all the spectrum estimation methods which are used later in this study.

## 2.1 Doppler Effect

The Doppler Effect is a very common physical phenomenon in our daily life. The most commonly used example to introduce the Doppler Effect may be that a police car is passing you with a howling alarm. You may hear the siren of the police car changing when it is passing you. The alarm sounds low when the car is behind you, and the alarm is rising when the car is approaching you. When the car has passed you, the alarm sounds reduced. The change of the sound is due to the change of the frequency of the sound wave. This phenomenon is called the Doppler Effect, and the changed frequency is the Doppler frequency.

The Doppler Effect was found by Austrian physicist, Christian Doppler, in 1842. When the sound source is moving away from the observer, the wavelength of the sound is increasing and the sound is turning down. On the contrary side, when the sound source is approaching the observer, the wavelength of the sound is decreasing and the sound is turning up.

The Doppler Effect is not only found in the sound wave, but also in other kinds of waves, for example, water waves, electromagnetic waves, etc. It is difficult to observe the Doppler Effect in electromagnetic wave without instruments. Here, take the sound wave as an example to analyze the Doppler Effect. Assume the sound source speed is $v_s$, the frequency of the sound source is $f_0$, the velocity of sound in the medium is c, the velocity of the observer is$v_r$, and the frequency of the observer is f.

There are four cases regarding the relationship between the source and the observer [1]:

**Case one: both source and observer hold still $v_s = v_r = 0$:**

$$f = f_0$$

**Case two: source holds still ($v_s = 0$), while observer moves:**

$$\mathrm{f} = \left(\frac{c \pm v_r}{c}\right) f_0 = (1 \pm \frac{v_r}{c}) f_0 \qquad (2.1)$$

"+" stands for observer approaches the source, while "-" stands for observer leaves the source.

**Case three: source moves, while observer holds still ($v_r = 0$):**

$$\mathrm{f} = (\frac{c}{c \mp v_s}) f_0 \qquad (2.2)$$

"+" stands for source leaves the observer, while "-" stands for source approaches the observer.

**Case four: both source and observer move:**

$$f = (\frac{c \pm v_r}{c \mp v_s}) f_0 \qquad (2.3)$$

"+" in the numerator and "-" in the denominator stand for source and observer approaching each other, while "-" in the numerator and "+" in the denominator stand for source and observer moving away from each other.

The equation reveals that:

$f > f_0$, when the observer is close to the source;

$f < f_0$, when the observer is away from the source;

The Doppler frequency is:

$$f_d = f - f_0$$

## 2.2 Doppler speed measurement principle

Figure 1 is a simple sketch to show the principle of the measurement. Radar is mounted face down on the front of the vehicle. The radar transmits microwaves to the surface of the road at point P and receives the reflected beam from point P. Assume the frequency of the radar is $f_0$.

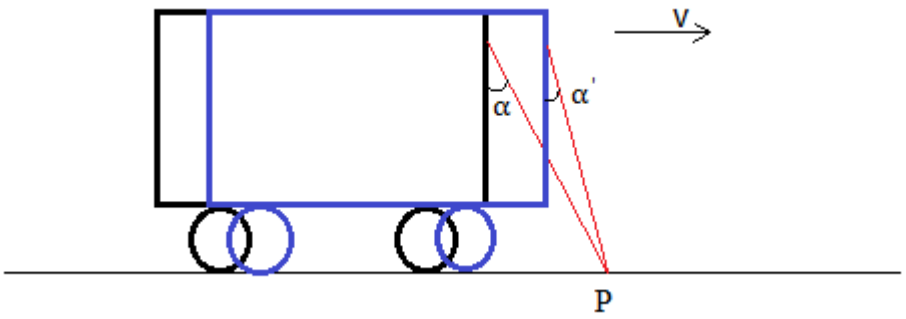


*Figure 1 - Vehicle radar working principle*

The frequency at point P can be calculated via Equation (2.2):

$$f_1 = \frac{c}{c - v\cos\alpha} f_0$$

To find the frequency of the beam reflected from P, the Equation (2.1) is needed:

$$f_2 = \left(1 + \frac{v\cos\alpha'}{c}\right) f_1 = \frac{c + v\cos\alpha'}{c - v\cos\alpha} f_0$$

The Doppler frequency is:

$$f_d = f_2 - f_0 = \frac{2v\cos\alpha'}{c - v\cos\alpha} f_0 \qquad (2.4)$$

The velocity of the microwave is $3.0\times 10^8 m/s$, which is so enormous that the velocity of the vehicle can be ignored. The angle change can be neglected.

$$\alpha \approx \alpha'$$

With the help of Taylor series, Equation (2.4) can be simplified as:

$$f_d = \frac{2v\cos\alpha}{c} f_0 \qquad (2.5)$$

In this equation, c, $\alpha$ and $f_0$ are already given, so the Doppler frequency $f_d$ is the key to obtaining the value of the velocity of the vehicle [2].

## 2.3 Doppler radar applications

Doppler radars are widely used in different areas. The working principle is the same as previously presented. Some examples of the applications of Doppler radar in other fields are listed below.

### 2.3.1 Doppler radar in weather prediction

Doppler radar can be used in weather prediction. The microwave is sent out and the radar station receives the reflected microwave. The Doppler radar observes the real time reflectivity factor, the mean radial velocity and the spectrum width. From this data information, people can predict disastrous weather like tornados, hail and flood [3].

### 2.3.2 Doppler radar for range measurement

Doppler radar can be used for range measurement. This application is widely used in ship or aircraft navigation, military target tracking and satellite relative applications, etc. These applications commonly employ the Range Doppler Algorithm [4]. A Doppler counter measures the total phase change. Each phase of the received signal slips one cycle relative to the phase of the transmitted signal, the distance over which the signal has increased by one wavelength. The Doppler counter thus provides a measure of range change over a count time [5][6].

### 2.3.3 Doppler radar in astronomy area

The Doppler Effect is used in the astronomy research area to measure the Doppler shift so that they can determine the orbits, radii and rotation vectors of the inner planets [7]. By measuring the distance to stars and their redshift and blueshift, astronomers are able to map the motion of our galaxy and get a picture of how our galaxy may look to an observer across the Universe [8].

## 2.4 Spectrum estimation methods

As the datasheet of the data module MDU2410 shows, the radar microwave unit consists of a homodyne transceiver. One path of the local oscillator is transmitted through an antenna, and the other path is fed to a mixer. The RF input of the mixer is connected to another antenna for receiving the reflected signal. The IF output (the

mixer product or quadrature I and output Q) is the input to the signal processor. Figure 2 shows the circuit descriptions of this radar module.

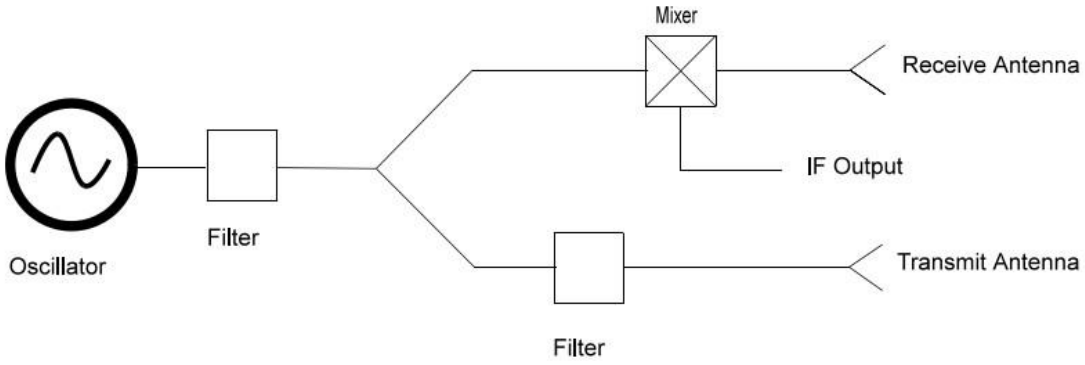


**Figure 2 – Radar *circuit descriptions [9]***

The IF signal can be expressed as the following equation:

$$x(t) = Ae^{i(2\pi f_d t+\theta)} \qquad (2.6)$$

The Doppler radar signal can be regarded as a stationary random signal in a very short time interval. To analyze this signal, spectrum estimation can be implemented.

The Doppler frequency estimation can be performed in both the time domain and the frequency domain. Analysis in the time domain is more intuitional because the signals change with respect to time, while the analysis in the frequency domain is easier to implement but not as intuitional as in the time domain. A given signal can be converted between the time domain and the frequency domain via Fourier transform, for example.

This thesis focuses on the analysis methods in the frequency domain. In these methods the frequency structure of the signals are analyzed to obtain the information, such as amplitude and frequency, of each component, which composes the signal. Spectrum estimation is the most commonly used way to calculate the spectrum of the received Doppler signal. By employing some algorithms, the spectrum which is responding to the velocity of the vehicle can be found out. Some classical spectrum estimation methods and modern spectrum estimation algorithms will be introduced respectively in the following sections.

### 2.4.1 Classical power spectrum estimation

The classical PSD estimations are easy to implement and understand. The common ground is that they are all based on the Fourier transform.

#### *2.4.1.1 The periodogram method*

One typical example is the periodogram method. It is a direct method to estimate the spectrum. Assume $x(n)$ is a random signal, the periodogram can be implemented in the following steps [10]:

a. Take N observations data $x_N(n)$ as the signal function.
b. Run the Fourier transform to get $X_N$.

$$X_N = \frac{1}{N}\sum_{n=0}^{N-1} x(n)\, e^{-j2\pi kn/N}$$

c. Square the amplitude and divide it by N.

$$P_{xx} = \frac{1}{N}\left|\sum_{n=0}^{N-1} x(n)\, e^{-j2\pi kn/N}\right|^2$$

In this way the power spectrum $P_{xx}$ of $x_N(n)$ was calculated. It can be done easily in Matlab, because in Matlab there is a built-in function "periodogram" which can directly return the power spectrum density estimation of the signal.

With the developing of fast Fourier transform (FFT), the periodogram is widely used to estimate the power spectrum, but the frequency spectrum resolution is low because all the other data besides the N observation data are regarded as zeros.

#### *2.4.1.2 Non-parametric methods*

Non-parametric methods are also classical methods, and they improve the periodogram. These methods make no assumption about how the data were generated and hence are called non-parametric. The typical non-parametric methods are the Bartlett method (1948), the Blackman and Tukey method (1958), and the Welch method (1967).

##### 2.4.1.2.1 The Bartlett Method

To reduce the variance in the periodogram, the Bartlett method involves three steps.

a. The N-point observation sequence is divided into K non-overlapping segments, where each segment has length M, N=KM.

$$x_i = x(n + iM), i = 0,1, \dots, K-1; n = 0,1, \dots M-1;$$

b. Compute the periodogram for each segment.

$$P_{xx}^{(i)}(f) = \frac{1}{M}\left|\sum_{n=0}^{M-1} x_i(n) e^{-j2\pi fn}\right|^2, i = 0,1, \dots, K-1$$

c. Take the average of the periodogram for the K segments to obtain the Bartlett power spectrum estimate.

$$P_{xx}^{B}(f) = \frac{1}{K}\sum_{i=0}^{K-1} P_{xx}^{i}(f)$$

There are both advantages and disadvantages in this method with respect to the periodogram. The advantage is that Bartlett's method reduces the variance of the Bartlett power spectrum estimate by factor K. The disadvantage is that it increases the deviation of each segment [11].

#### 2.4.1.2.2 The Welch Method

The Welch method made two basic modifications to the Bartlett method. For the first, it allowed the segments to overlap and for the second modification, it used a window to filter the data before computing the periodogram. The Welch method is followed in three steps:

a. Overlapped segments

$$x_i(n) = x(n + iD), n = 0,1, \dots, M-1; i = 0,1, \dots, L-1;$$

In this expression, $iD$ is the starting point for the ith sequence. Observe that if D= M, the segments do not overlap and the number L of data segments is identical to the number K in the Bartlett method. If D = M/2, for instance, there is 50% overlap between successive data segments and L = 2K segments are obtained.

b. Window the data before computing the periodogram.

$$P_{xx}^{(i)}(f) = \frac{1}{MU}\left|\sum_{n=0}^{M-1} x_i(n)\omega(n)e^{-j2\pi fn}\right|^2, i = 0,1, \dots, L-1$$

In this expression, U is a normalization factor for the power in the window function and is selected as:

$$U = \frac{1}{M}\sum_{n=0}^{M-1} \omega^2(n)$$

c. The Welch power spectrum estimate is the average of these modified periodograms:

$$P_{xx}^{W}(f) = \frac{1}{L}\sum_{i=0}^{L-1} P_{xx}^{(i)}(f)$$

The Welch method improves the Bartlett method. Both the Bartlett method and the periodogram compute the power spectrum and then implement the window to modify the result. The Welch method implements the window function to weight the segments at first. By doing this, it reduces the correlation between each segment. Additionally, the overlap can make full use of the data so that even less data can lead to a good result. As a result the Welch method can control the variance of the power spectrum estimation [12].

#### 2.4.1.2.3 The Blackman and Tukey Method

The Blackman and Tukey method was developed by Blackman and Tukey in 1958. This method is also called the BT method or the autocorrelation method. In this method the sample autocorrelation sequence is windowed first and then Fourier transformed to obtain the power spectrum estimation. It is an indirect method to obtain the power spectrum estimation and can be presented by the two steps below.

a) Estimate the autocorrelation function:

$r_{xx}(m) = E[x^*(n)x(n+m)] = \frac{1}{N}\sum_{n=0}^{N-1} x(n+k)x^*(n)$, k = 0,1,2,⋯, M

b) Run Fourier transform of $r_{xx}(m)$ and get the power spectrum estimation:

$$P_{xx}^{BT}(f) = \sum_{m=-(M-1)}^{M-1} r_{xx}(m)\omega(m)e^{-j2\pi fm}$$

The purpose of the window is to smooth the periodogram estimate, thus to decrease the variance in the estimate at the expense of reducing the resolution [13].

The Welch and BT PSD spectrum estimates are somewhat better than the Bartlett estimate. However, the differences in performance are relatively small. Because the Welch method is widely used in engineering applications, it is selected for a further analysis in the later discussion [14].

### 2.4.2 The selection of window functions.

As presented previously, the Welch method windowed each segment prior to computing the periodogram. There are some frequently used window functions in digital signal processing. This section discusses the characteristics of the most used window functions.

Table 1 below introduces the five most used window functions and their expressions in the time domain [15].

*Table 1 – Five window functions*

| Type of window | Sequence expression in time domain |
|---|---|
| Rectangle | 1 |
| Bartlett | $\begin{cases} \frac{2n}{N-1}, 0 \le n \le \frac{N-1}{2} \\ 2-\frac{2n}{N-1}, \frac{N-1}{2} \le n \le N-1 \end{cases}$ |
| Hanning | 0.5-0.5cos($\frac{2\pi n}{N-1}$) |
| Hamming | 0.54-0.46cos($\frac{2\pi n}{N-1}$) |
| Blackman | 0.42-0.5cos($\frac{2\pi n}{N-1}$)+0.08($\frac{4\pi n}{N-1}$) |

Table 2 below shows the important frequency domain characteristics [15].

*Table 2 – Characteristics of windows*

| Type of window | Width of main lobe | Peak side lobe (dB) |
|---|---|---|
| Rectangle | $\frac{4\pi}{N}$ | -13 |
| Bartlett | $\frac{12\pi}{N-1}$ | -25 |
| Hanning | $\frac{8\pi}{N-1}$ | -31 |
| Hamming | $\frac{8\pi}{N-1}$ | -41 |
| Blackman | $\frac{8\pi}{N-1}$ | -57 |

It is obvious that the Rectangle window is the simplest window. The advantage of the Rectangle window is that the main lobe is concentrated, while the disadvantage is that the side lobes are quite high, as shown below in Figure 3.

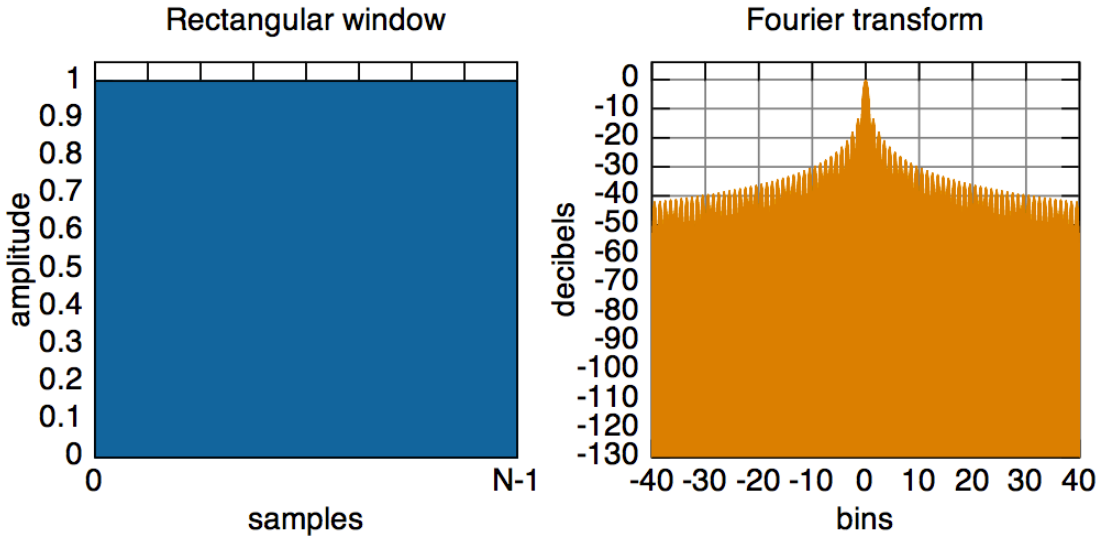


*Figure 3- Rectangular window [16]*

The Bartlett window shown in Figure 4 is also called the triangular window. This window can be seen as the convolution of two half-sized rectangular windows (for N even). Compared to the rectangular window, the main lobe width of this window is about double the main lobe width of the rectangular window. The side lobes are much smaller than the side lobes of the rectangular window.

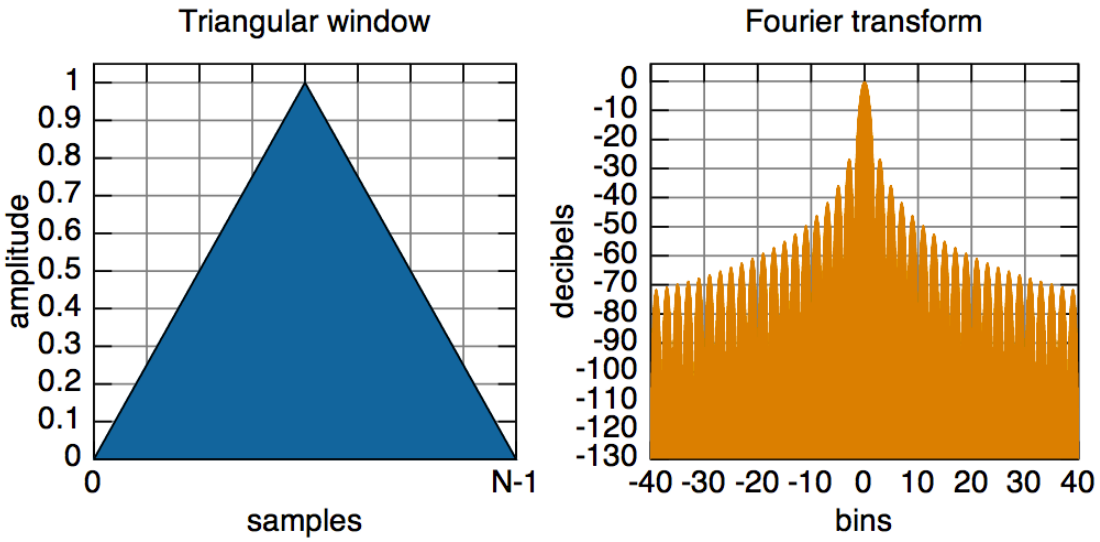


*Figure 4 - Triangular window [16]*

The Hanning (or Hann) window shown in Figure 5 can be seen as the summation of three rectangular windows [15].

$$\omega(n) = \frac{1}{2}\omega_r(n) + \frac{1}{4}e^{i2\pi\frac{n}{N-1}}\omega_r(n) + \frac{1}{4}e^{-i2\pi\frac{n}{N-1}}\omega_r(n)$$

The advantage of the Hanning window is very low aliasing. Compared to the rectangular window, the main lobe of the Hanning window is wider but smaller. The side lobes decrease obviously and fast. Refer to Figure 5.

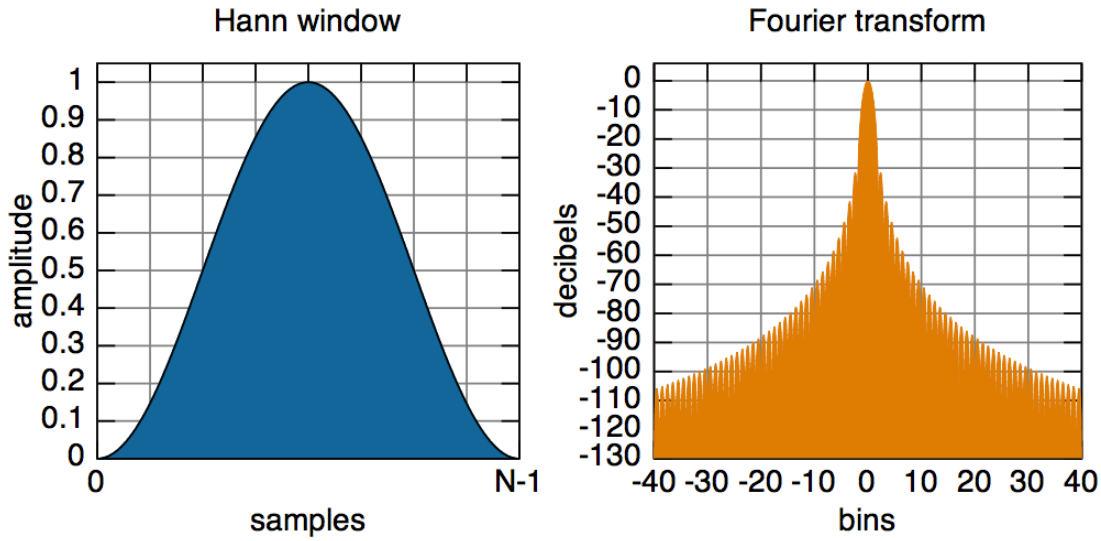


*Figure 5 - Hanning window [16]*

The Hamming window is also a kind of cosines window, the same as the Hanning window, and the only difference is the weighted factor, which makes the side lobes lower, but attenuation is slower than in the Hanning window. It is displayed in Figure 6.

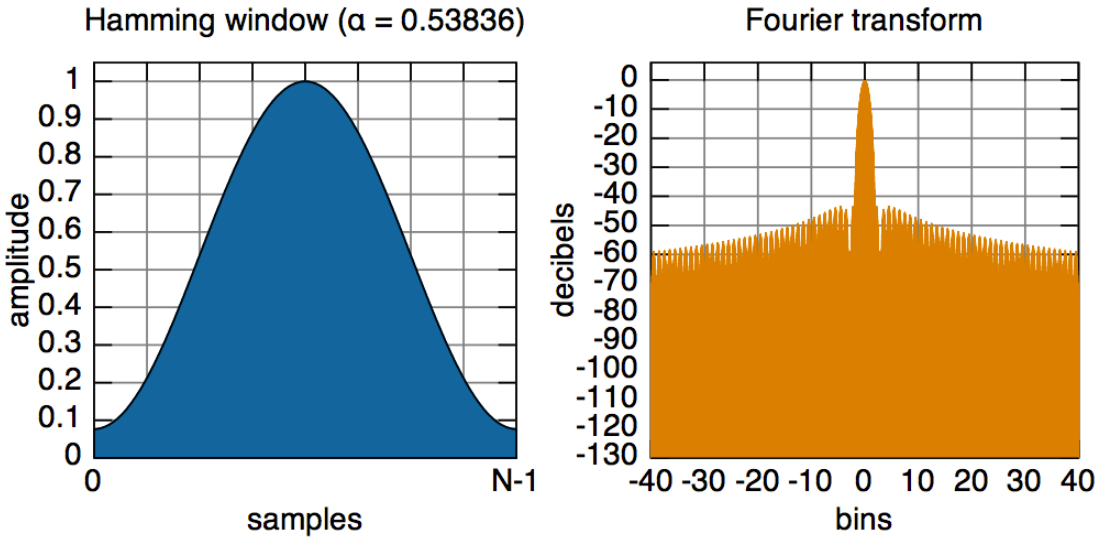


*Figure 6 - Hamming window [16]*

The Blackman window is the narrowest among these five windows, and the side lobes attenuate fastest, while the transition band is the widest. It is shown in Figure 7.

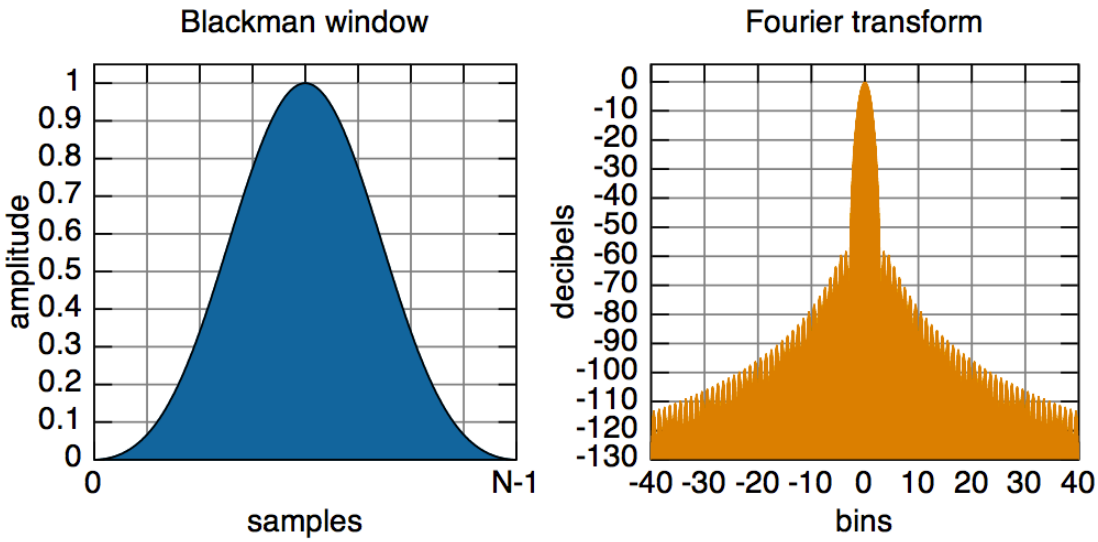


*Figure 7 - Blackman window [16]*

All the windows have both advantages and disadvantages, and the window selection is a tradeoff between the pass band ripple and transition band steepness. The key is to consider the characteristics of the signal and the request regarding the signal processing. For example, if the only request is for high resolution, the rectangular window is an appropriate choice because it has a narrow main lobe, and, on the other hand, if the signal has a strong noise, it is better to select the window which has lower side lobes and fast attenuation.

### 2.4.3 Parametric methods

This section introduces another kind of spectrum estimation method: parametric methods for power spectrum estimation. The classical FFT-based PSD estimation methods assume all the data besides the sampled data are zeros, so that the frequency resolution is relatively low. The parametric methods do not require such an assumption. In these methods, the random sequence is regarded as a signal from a signal source with specific parameters and structures. By selecting a proper model, it is possible to calculate the parameters of the model from the sampled data, and then calculate the data besides the window, instead of regarding them as zeros. The key of these methods is to select a proper model and work out the parameters of the model. Once the parameters of the model are determined, the original signal from the signal source can be estimated. Furthermore, the PSD can be estimated. The parametric methods make up the limits of the classical PSD estimation methods.

#### *2.4.3.1 Parametric models*

The parametric methods are approached in three steps:

1. Select a suitable parametric model.

2. Determine the parameters for the model from the sampled data.

3. Take the parameters back to the selected model and calculate the PSD estimation.

Suppose the data sequence $x(n)$ is the output of a linear system $H(z)$ impulse by an input sequence $u(n)$. No matter whether the sequence $x(n)$ is a random signal or not, there is a relation between the input sequence $u(n)$ and the output sequence $x(n)$ [17].

$$x(n) = -\sum_{k=1}^{p} a_k x(n-k) + \sum_{k=0}^{q} b_k u(n-k)$$

$$x(n) = \sum_{k=0}^{\infty} h(k)u(-n)$$

Take the Z-transform for both sides of the above two equations; suppose $b_0 = 1$ [18].

$$H(z) = \frac{B(z)}{A(z)}$$

where

$$A(z) = 1 + \sum_{k=1}^{p} a_k z^{-k}$$

$$B(z) = 1 + \sum_{k=1}^{q} b_k z^{-k}$$

$$H(z) = \sum_{k=0}^{\infty} h(k) z^{-k}$$

Only, and if only, both the zeros of $A(z)$ and $B(z)$ are in the unit circle, the system $H(z)$ is a stable minimum phase system [18].

Suppose the variance of the white noise sequence $u(n)$ is $\sigma^2$, and the power spectrum of the output sequence $x(n)$ is:

$$P_x\left(e^{j\omega}\right) = \frac{\sigma^2 B\left(e^{j\omega}\right) B^*(e^{j\omega})}{A^*(e^{j\omega}) A(e^{j\omega})} = \frac{\sigma^2 \left|B(e^{j\omega})\right|^2}{|A(e^{j\omega})|^2}$$

This equation reveals that if the variance of the white noise $\sigma^2$ and the parameters of the model $a_1, a_2, \cdots, a_p, b_1, b_2, \cdots, b_q$ are known, the power spectrum can be determined.

Divide the output sequence into three cases:

1) All the $b_1, b_2, \cdots, b_q$ are zeros:

$$x(n) = -\sum_{k=1}^{p} a_k x(n-k) + u(n)$$

$$H(z) = \frac{1}{A(z)} = \frac{1}{1 + \sum_{k=1}^{p} a_k z^{-k}}$$

$$P_x\left(e^{j\omega}\right) = \frac{\sigma^2}{A^*(e^{j\omega})A(e^{j\omega})} = \frac{\sigma^2}{\left|1 + \sum_{k=1}^{p} a_k z^{-k}\right|^2}$$

This is the autoregressive (AR) model.

2) All the $a_1, a_2, \cdots, a_p$ are zeros:

$$x(n) = u(n) + \sum_{k=0}^{q} b_k u(n-k)\,, b_0 = 1$$

$$H(z) = B(z) = 1 + \sum_{k=1}^{q} b_k z^{-k}$$

$$P_x\left(e^{j\omega}\right) = \sigma^2 B\left(e^{j\omega}\right) B^*(e^{j\omega}) = \sigma^2 \left|1 + \sum_{k=1}^{q} b_k z^{-k}\right|^2$$

This is the moving-average (MA) model.

3) None of $a_1, a_2, \cdots, a_p, b_1, b_2, \cdots, b_q$ are zeros:

$$x(n) = -\sum_{k=1}^{p} a_k x(n-k) + \sum_{k=0}^{q} b_k u(n-k)$$

This is called the autoregressive moving average (ARMA) model.

The AR model is the most widely used among these three linear models. There are two main reasons. For the first, the AR model is suitable for representing spectra with narrow peaks. Secondly, the AR model results in very simple linear equations for the AR parameters. On the other hand, the MA model, as a general rule, requires many more coefficients to represent a narrow spectrum. Consequently, it is rarely used by itself as a model for spectrum estimation.

Wold's (1938) decomposition theorem asserts that any ARMA or MA process can be represented uniquely by an AR model of possibly infinite order, and any ARMA or AR process can be represented by an MA model of possibly infinite order [17]. In view of this theorem, the issue of model selection is reduced to selecting the model that requires the smallest number of parameters that are also easy to compute. The AR model is selected in this thesis.

### 2.4.3.2 AR model

The output data sequence of the AR model is:

$$x(n) = -\sum_{k=1}^{p} a_k x(n-k) + u(n)$$

where the sequence $u(n)$ is the white noise, p is the order, $a_k$ is the parameter of the AR model.

The power spectrum of the sequence $x(n)$ is:

$$P_{xx}(e^{j\omega}) = \frac{\sigma^2}{A^*(e^{j\omega})A(e^{j\omega})} = \frac{\sigma^2}{\left|1 + \sum_{k=1}^{p} a_k z^{-k}\right|^2}$$

where $\sigma^2$is the variance of the white noise.

If the parameters $a_k(k = 1,2,\cdots,p)$ and the variance $\sigma^2$ are determined, the power spectrum estimation can be figured out. Before this we shall take a look at the relationship between the parameters and the autocorrelation sequence.

When the power spectral density of the stationary random process is a rational function, there is a basic relationship between the autocorrelation sequence $\gamma_{xx}(m)$ and the parameters $a_k$ and $b_k$ of the linear filter $H(z)$ that generates the process by filtering the white noise sequence $u(n)$. This relationship can be approached by multiplying the difference equation of $x(n)$ by $x^*(n-m)$ and taking the expected value of both sides of the resulting equation [19].

$$E[x(n)x^*(n-m)] = -\sum_{k=1}^{p} a_k\, E[x(n-k)x^*(n-m)]$$

$$+\sum_{k=0}^{q} b_k\, E[u(n-k)x^*(n-m)]$$

Hence:

$$\gamma_{xx}(m) = -\sum_{k=1}^{p} a_k \gamma_{xx}(m-k) + \sum_{k=0}^{q} b_k\, \gamma_{ux}(m-k)$$

where $\gamma_{xx}(m)$ is the cross correlation sequence between $u(n)$ and $x(n)$.

The cross correlation $\gamma_{ux}(m)$ is related to the filter impulse response. That is,

$$\gamma_{ux}(m) = E[x^*(n)u(n+m)] = E\left[\sum_{k=0}^{\infty} h(k)u^*(n-k)u(n+m)\right] = \sigma^2 h(-m)$$

where, in the last step, the sequence $u(n)$ is white. Hence:

$$\gamma_{ux}(m) = \begin{cases} 0, & m \geq 0 \\ \sigma^2 h(-m), & m \leq 0 \end{cases}$$

The desired relationship is:

$$\gamma_{xx}(m) = \begin{cases} -\sum_{k=1}^{p} a_k \gamma_{xx}(m-k), & m > q \\ -\sum_{k=1}^{p} a_k \gamma_{xx}(m-k) + \sigma_u^2 \sum_{k=0}^{q-m} h(k) b_{k+m}, & 0 \leq m \leq q \\ \gamma_{xx}^*(-m), & m < 0 \end{cases}$$

This represents a nonlinear relationship between $\gamma_{xx}(m)$ and the parameters $a_k$ and $b_k$, and the relationship applies to the ARMA process. For an AR process, we can simplify to:

$$\gamma_{xx}(m) = \begin{cases} -\sum_{k=1}^{p} a_k \gamma_{xx}(m-k), & m > 0 \\ -\sum_{k=1}^{p} a_k \gamma_{xx}(m-k) + \sigma_u^2 \sum_{k=0}^{q-m} h(k) b_{k+m}, & m = 0 \\ \gamma_{xx}^*(-m), & m < 0 \end{cases}$$

Thus we have a linear relationship between $\gamma_{xx}(m)$ and the parameter $a_k$. These equations can be expressed in the matrix form

$$\begin{bmatrix} \gamma_{xx}(0) & \gamma_{xx}(-1) & \gamma_{xx}(-2) & \cdots & \gamma_{xx}(m) \\ \gamma_{xx}(1) & \gamma_{xx}(0) & \gamma_{xx}(-1) & \cdots & \gamma_{xx}(m) \\ \vdots & \vdots & \vdots & & \vdots \\ \gamma_{xx}(p) & \gamma_{xx}(p-1) & \gamma_{xx}(p-2) & \cdots & \gamma_{xx}(m) \end{bmatrix} \begin{bmatrix} 1 \\ a_1 \\ \vdots \\ p \end{bmatrix} = \begin{bmatrix} \sigma_u^2 \\ 0 \\ \vdots \\ 0 \end{bmatrix}$$

These equations are Yule-Walker equations. It is obvious that it is simple to calculate the parameters of the AR model when we know the autocorrelation of the observation data sequence, and thus the power spectrum of the signal can be figured out [19].

#### *2.4.3.3 Methods based on the AR model*

This section introduces three methods based on the AR model. These methods are the Levinson-Durbin method, Burg method and Marple method.

1. The Levinson-Durbin method
   The Levinson-Durbin method is an efficient method for predicting the coefficients in the normal equation of $\gamma_{xx}(m)$. The heart of this method is to exploit the special symmetry in the autocorrelation matrix. Note that the autocorrelation matrix is a Toeplitz matrix [20][21].

$$R_p = \begin{bmatrix} \gamma_{xx}(0) & \gamma_{xx}(-1) & \gamma_{xx}(-2) & \cdots & \gamma_{xx}(m) \\ \gamma_{xx}(1) & \gamma_{xx}(0) & \gamma_{xx}(-1) & \cdots & \gamma_{xx}(m) \\ \vdots & \vdots & \vdots & & \vdots \\ \gamma_{xx}(p) & \gamma_{xx}(p-1) & \gamma_{xx}(p-2) & \cdots & \gamma_{xx}(m) \end{bmatrix}$$

where $R_p(i,j) = R_p(j,i)$.

It begins with a predictor of order m=1, and then increases the order recursively, using the lower order solutions to obtain the solution to the next-higher order. Thus the solution to the first-order predictor is:

$$a_1 = -\frac{\gamma_{xx}(1)}{\gamma_{xx}(0)}$$

and the resulting MMSE is

$$\mathrm{E}_1^{\mathrm{f}} = \gamma_{\mathrm{xx}}(0) + \mathrm{a}_1(1)\gamma_{\mathrm{xx}}(-1) = \gamma_{\mathrm{xx}}(0)[1 - |\mathrm{a}_1(1)|^2]$$

then increase the order m =2 and calculate the coefficient $\mathrm{a}_2(1)$, $\mathrm{a}_2(2)$ and so on until all the coefficients are calculated when $\mathrm{m} = \mathrm{p}$.

2. The Burg method

The method devised by Burg (1968) for estimating the AR parameters can be viewed as an order-recursive least-squares lattice method, based on the minimization of the forward and backward errors in linear predictors, with the constraint that the AR parameters satisfy the Levinson-Durbin recursion. Suppose that there is an N data sequence $\mathrm{x}(0), \mathrm{n} = 0, \cdots, \mathrm{N}-1$. The Burg method is approached in the following steps [22]:

a. Take m=1, initialize: $\mathrm{e}_0^{\mathrm{f}}(\mathrm{n}) = \mathrm{e}_0^{\mathrm{b}}(\mathrm{n}) = \mathrm{x}(\mathrm{n}), \mathrm{n} = 0,1, \cdots, \mathrm{N}-1$

$$\sigma_0^2 = R(0) = \frac{1}{N}\sum_{n=0}^{N-1} x^2(n)$$

b. Calculate the reflection coefficient:

$$k_m = \frac{-2\sum_{n=m}^{N-1} e_{m-1}^f(n) e_{m-1}^b(n-1)}{\sum_{n=m}^{N-1}\left[(e_{m-1}^f(n))^2 + (e_{m-1}^b(n-1))^2\right]}$$

c. Calculate the coefficient of the lattice filter and predict the error of power:

$$a_m(m) = k_m$$

$$a_m(k) = a_{m-1}(k) + k_m a_{m-1}(m-k), k = 1,2, \cdots, m-1$$

$$E_m = \sigma_m^2 = (1 - k_m^2)E_{m-1}$$

d. Calculate recursively the higher order forward and backward prediction error:

$$e_m^f(n) = e_{m-1}^f + k_m e_{m-1}^b(n-1)$$

$$e_m^b(n) = e_{m-1}^b + k_m e_{m-1}^f(n)$$

e. Update m to m + 1, repeat steps from b) to d) until m = p

There are three major advantages of the Burg method for estimating the parameters of the AR model:

a) It results in high frequency resolution.
b) It yields a stable AR model.
c) It is computationally efficient.

However, this method is known to have some limitations, such as line splitting, spurious peaks and frequency bias [23].

3. The Marple method

This method, which is also called the modified covariance method, was developed by Larry Marple in 1980. There are some superiorities of this method with respect to the Burg method. The resolution is better, the data sequence can be shorter and the anti-interference ability is stronger. Because of these advantages, the Marple method was widely used.

The Marple method provides the exact least squares solution, without matrix inversion, for the AR parameter estimates outlined. The Levinson-Durbin recursion constraint is removed.

$$\varepsilon_p = \sum_{n=p}^{N-1} \left\{ \left[ e_p^f(n) \right]^2 + \left[ e_p^b(n) \right]^2 \right\}$$

$$= \sum_{n=p}^{N-1} [\sum_{k=0}^{p} a_p(k) x(n-k)]^2 + \sum_{n=p}^{N-1} [\sum_{k=0}^{p} a_p(k) x(n+k-p)]^2 ,$$

$$a_p(0) = 1$$

Derivate this equation with respect to each predicted coefficient $a_p(k)$, and then take the obtained equation equal to zero; the result is a group of linear equations. The optimal predicted coefficient $a_p(k)$ can be obtained by solving these linear equations.

Marple gave an efficient recursive algorithm, which is a lattice structure and thus can reduce calculations [24].

# 3. Modeling

This chapter introduces the modeling of this system. A geometric model is built to simulate the radar radiation area. The equations presented in the previous chapter are used here to calculate the Doppler frequency. As a result of the modeling, the power spectrum density (PSD) is worked out. This spectrum is ideal because it is calculated based on the theoretical data. It is used to estimate the feasibility of the model. Furthermore it is used to compare with the real measured signal's spectrum.

## 3.1 Radar coverage pattern

According to the datasheet of Radar module MDU2410, the -3 dB beam width of this radar module is 72° horizontally and 36° vertically, respectively. The radar coverage pattern is shown in Figure 8 below [25].

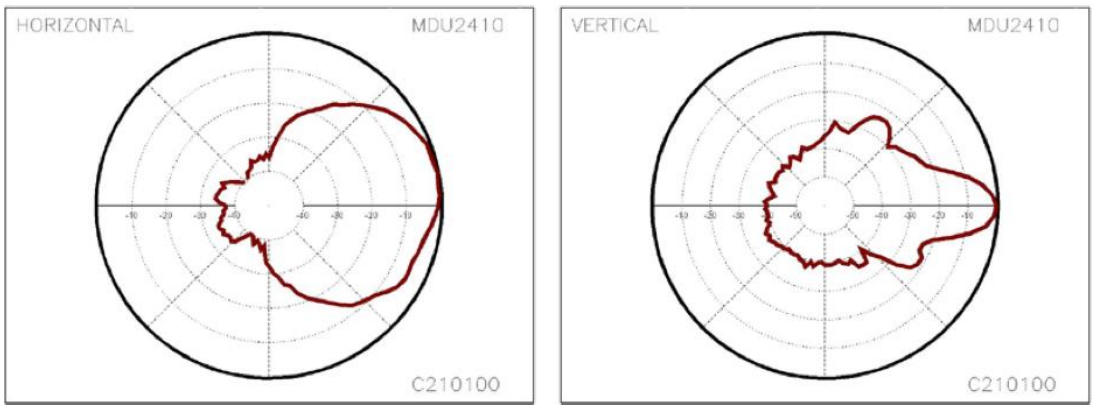


*Figure 8 - Radar coverage pattern [25]*

The radar module should be fixed on the front window of the vehicle. To obtain a better back-reflected signal, the radar should be fixed at 45 degrees [2] between the vertical lines facing down to the road. If this angle was too small, the radar would receive most of the signal reflected by the vehicle itself, because of the engine bonnet. If this angle was too wide, the reflected signal would be weak, because the distance increases greatly when the angle is getting wider and wider. The modified radar pattern in vertical plane is shown in Figure 9.

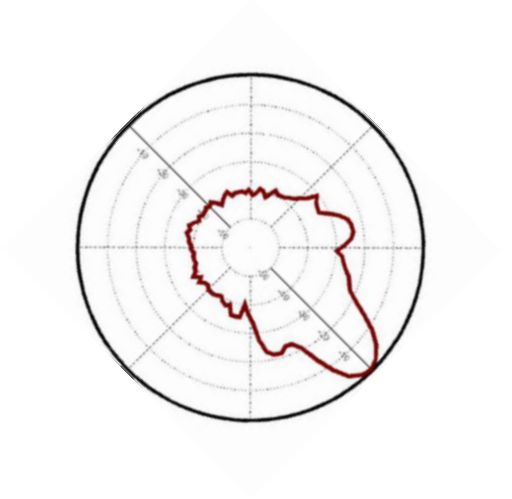

*Figure 9 – Main lobe in vertical plan*

Figure 10 below shows a 3D coordinate system. Point A in the sketch is the position where the radar module is supposed to fix on the vehicle. Point H is the origin of the coordinate system. The red line in the sketch is the axis of the main lobe of the radar signal, which is 45 degrees between the Y-axis down face to the XZ plane. The XZ plane stands for the road surface. The shadowed area in the middle of the XZ plane responds to the -3 dB beam width of the radar signal. It is the radiation area from which the strongest reflected energy comes. Besides this shadowed area, the radar also receives a back-reflected signal due to the side lobes, but they are relatively weak compared with the signal reflected from the shadowed area. The two curves in the XY plane show the boundary of the radiation area. The shape of the radiation area on the road surface is not important, because the integral thought implemented here is to calculate the reflected power from the road. The total reflected power is regarded as the summation of thousands of small grids on the road. Observing the radar coverage pattern in the horizontal plane, it can approximately be seen as symmetry about the X-axis. Thus the 3D coordinate system can be simplified as just a half part, as shown in Figure 10. Calculate the reflected power in the half part XZ plane and then double it to get a final value. The simplified coordinate system is shown in Figure 11.

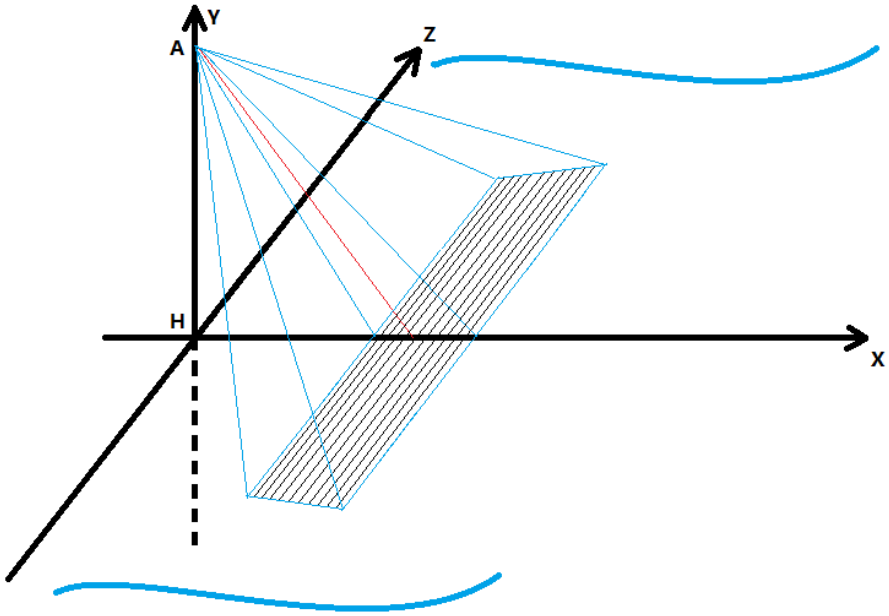


*Figure 10 - 3D coordinate system*

Viewed from the integral aspect, the radiation area can be divided into thousands of small square grids. The reflected power and Doppler frequency from each of these small grids can be calculated and the summation of them is the total reflected power with respect to the Doppler frequency in this area. To get a final result, the total reflected power should be doubled on account of the reflected power from the negative half part of the XZ plane. The direction of the vehicle is shown in Figure 11, along the positive X-axis. The height of the radar module is supposed to be 2 m at the beginning, and it can be modified later in the system code. Suppose the radar signal incident angle range is from 0 to 80 degrees [2]. The signals with incident angle over 80 degrees shall go through a long distance so that the reflected signal can be ignored. The two red lines AK and AJ are supposed to be the boundary of the radar signal on the X-axis and Z-axis direction, respectively, which means that the angle between the Y-axis and each red line AK and AJ is 80 degrees, although they looked as if they were too short in Figure 11. Point P is the center point of one grid. The computations begin with the distance from the radar to point P, and this value is the distance from the radar to the grid. Consequently, the smaller and the more numerous the grids are, the more precise the result is.

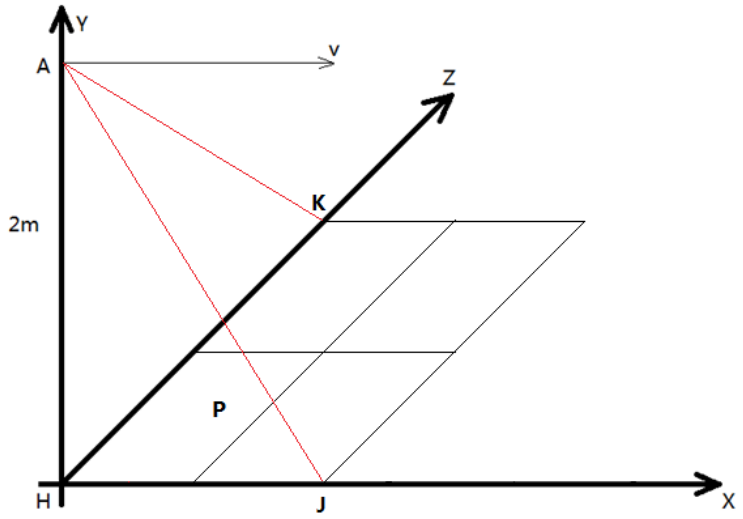


*Figure 11 - Simplified coordinate system*

Figure 12 below illustrates how the geometric model looked based on the simplified coordinate system in Figure 11. The line segment NP is vertical to the plane XZ and the line segment MQ, and the line segment PQ is vertical to the X-axis. It is obvious that the length of line segment HQ and the length of the line segment PQ stand for the coordinates of the point P (x, y). Two angles, $\alpha$ and $\beta$, are shown in Figure 12. Angle $\alpha$ represents the angle between the direction of the vehicle and the radar incident signal to this grid, which is line segment AP in this sketch. Angle $\beta$ is the incident angle of the radar beam, and the range is from 0 to 80 degrees, as presented before. With the help of this geometric model, the useful data like the angles and the distance from radar to each grid can be worked out. These data should be used in the later computations to find out the Doppler frequency and the reflected power.

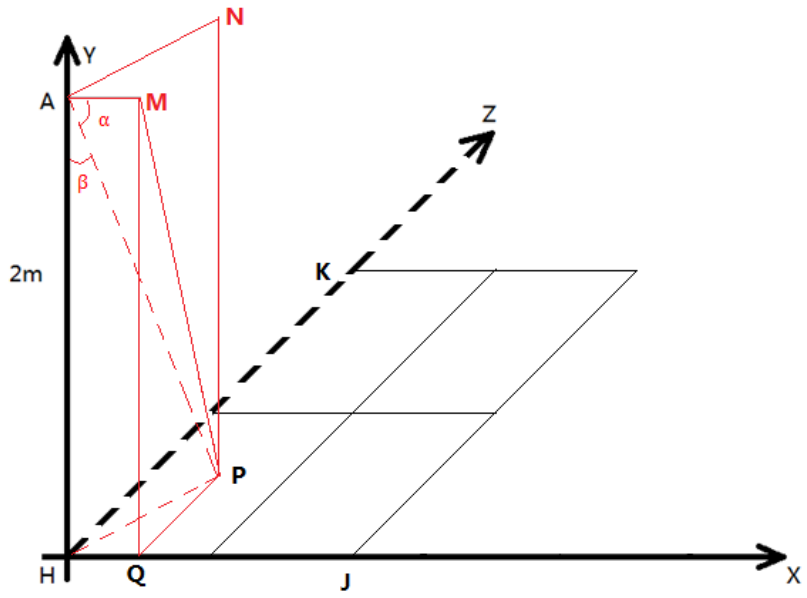


*Figure 12 - Geometric model*

The line segment AH is supposed to be 2 m here in this geometric model. The height of the radar can be adjusted later in the practical measuring. Point K and Point J are the critical points when the radar incident signal is 80 degrees. The length of HJ and HK is:

$$HJ = HK = AH * \tan(80°) \cong 11.34m$$

At the beginning, the radiation area is divided into four square-grids, then the length of HQ and PQ is a quarter of the length of HJ:

$$HQ = PQ = \frac{1}{4} \times HJ = 2.835m$$

Angle $\alpha$ and angle $\beta$ can be found with the help of the Cosine law and the Pythagorean Theorem. Angle $\alpha$ is in triangle MAP, and angle $\beta$ is in triangle PAH.

To calculate angle $\alpha$, it is necessary to find out the length of each side.

$$MP = \sqrt{MQ^2 + PQ^2} = \sqrt{2^2 + 2.835^2} \cong 3.469$$

$$AP = \sqrt{AH^2 + HQ^2 + PQ^2} = \sqrt{2^2 + 2.835^2 2.835^2} \cong 4.48$$

$$\mathrm{AM} = \mathrm{HQ} = 2.835$$

According to the Cosine law, angle $\alpha$ is:

$$\cos\alpha = \frac{AM^2 + AP^2 + MP^2}{2 \times AP \times AM} = \frac{2.835^2 + 4.48^2 - 3.469^2}{2 \times 4.48 \times 2.835} \cong 0.633$$

$$\alpha = cos^{-1}(0.633) \cong 50.728°$$

Angle $\beta$ is in triangle ΔHAP:

$$\cos\beta = \frac{AH}{AP} = \frac{2}{4.48} \cong 0.446$$

$$\beta = cos^{-1}(0.446) \cong 63.512°$$

So far the three important pieces of data in this model have been found. The next step is to repeat the same computations in each grid and find out the three items of data for each grid. The iteration can be done by a for-loop with the Matlab code.

## 3.2 Power density estimation

The radar module employed in this thesis is MDU2410, which has been developed by Microwave Solutions Ltd. The operating frequency is 24 GHz, and the sensitivity is -76 dBm with 10 dB S/N ration. The maximum transmitted power is 5 mW.

The power, which is transmitted in all directions, gives a power density back at the MDU, which can be calculated by the formula below [25]:

$$P_d = P_t \sigma G \frac{1}{(4\pi R^2)^2} \quad (3.1)$$

where:

| | | | | |
|---|---|---|---|---|
| Wavelength | $\lambda$ | = | 1.24cm | (.0124) |
| Transmit Power | $P_t$ | = | 5mW | (.005) |

The antenna gain can be found by summing the vertical gain value and the horizontal gain value in dB at this point.

If the $\sigma$ in the equation above was known, which stands for the radar cross-section of the road, it would be possible to calculate the reflected power. The strength of the backscattered signal from the road surface is difficult to predict deterministically [26]. It varies with the condition of the road and the angle of the incidence of signal. We found a relevant journal article, "Automotive Radar Technology for Detecting Road Conditions Backscattering Properties of Dry, Wet, and Icy Asphalt" [27], which presented the methods of measuring the RCS of asphalt with dry, wet and icy road surface. We can refer to the result in this thesis, but it will introduce errors in our final result, because the referred thesis is based on the USA road building standard, while our measurement is based on the Norwegian standard. Additionally, the RCS is sensitive to the temperature and the material of the road surface [27]. The deviation of the RCS selection will introduce the errors into the results, but this referenced thesis is the only one showing the result of RCS of asphalt that we can find in plenty of theses. Figure 13 shows the result of backscattering coefficient $\sigma_0$ of the asphalt road surface, which is extracted from the paper. The relation between the RCS and the $\sigma_0$ is:

$$\sigma = \text{Area} \times \sigma_0 \quad (3.2)$$

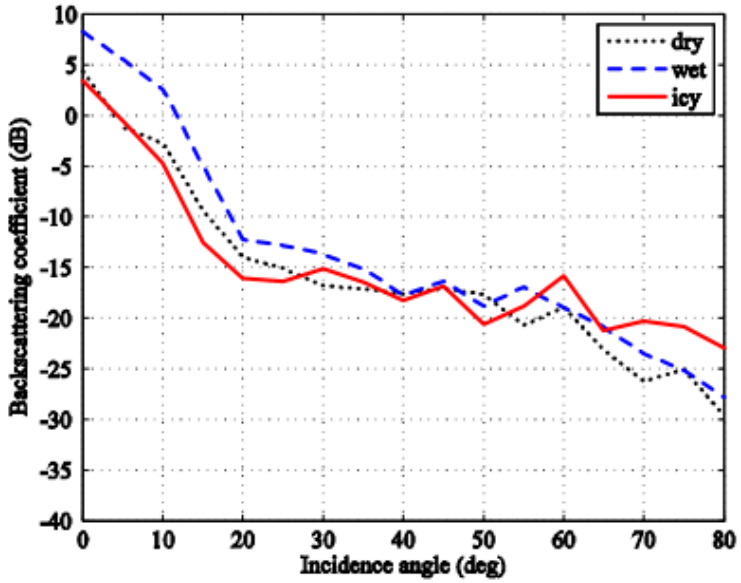


*Figure 13 - Backscattering coefficient (dB)*

The curves in Figure 13 are picked from journal article [27]. They illustrate that the backscattering coefficient $\sigma_0$ reduces when the incident angle increases, no matter whether the road surface is dry, wet or icy. The $\sigma_0$ keeps relatively steady when the incident angle is between 30 and 50 degrees. Outside this range the $\sigma_0$ drops significantly. In the geometric model, the incident angle of the radar beam to each grid varies. It is not accurate to adopt one value of the backscattering coefficient in all the calculations. To obtain as precise a result as possible, it is necessary to read the backscattering coefficient from the curves with respect to different incident angles. In the previous computations, the incident angle of each grid has been found. Figure 14 below shows the simulated backscattering coefficient curve in Matlab so that each incident angle has a responding backscattering coefficient value.

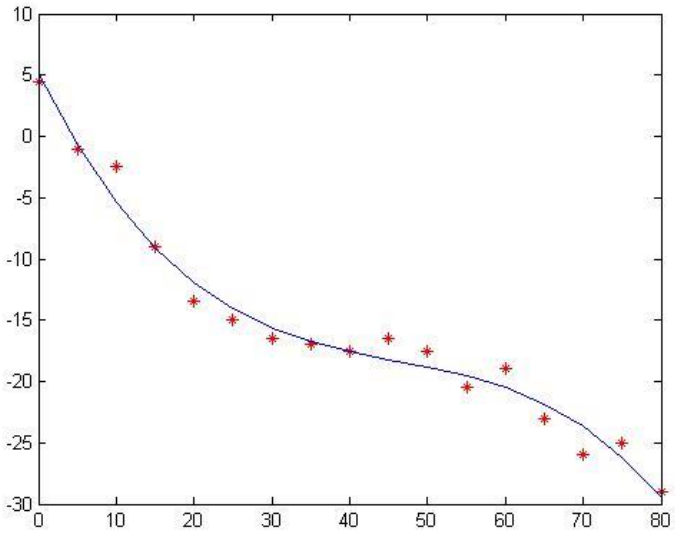


*Figure 14 - Simulated $\sigma_0$ curve*

The relation between the RCS and the $\sigma_0$ is shown in Equation (3.2), so that each RCS of each grid can be calculated. The reflected power of each grid can be found with the help of Equation (3.1). The sum of the reflected power from these grids is the total reflected power.

Equation (2.5) gives the relation between the Doppler frequency and the angle α:

$$f_d = \frac{2v\cos\alpha}{c} f_0$$

The Doppler frequency of each grid can be worked out from this equation.

All the calculations were done in Matlab. The radiation area was divided into $64 \times 64$ grids, $128 \times 128$ grids and $256 \times 256$ grids, respectively. Supposing the vehicle was travelling at 10 km/h, the simulation results are shown below.

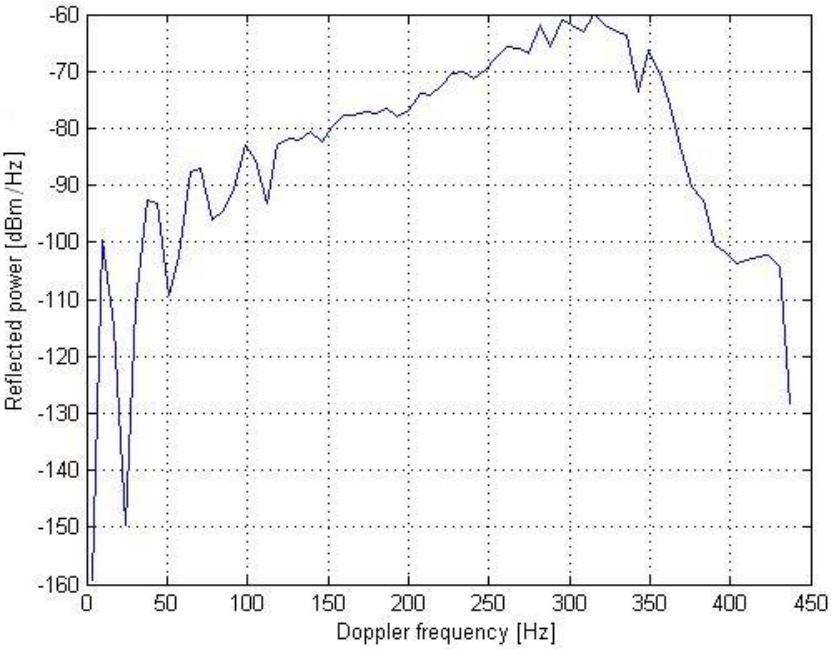


*Figure 15 - 64*64 grids*

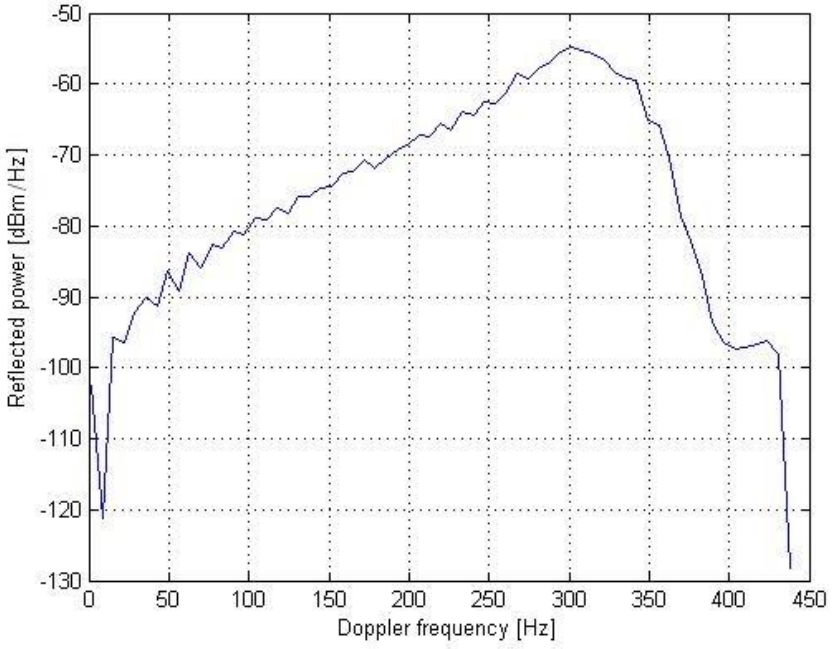


*Figure 16 - 128*128 grids*

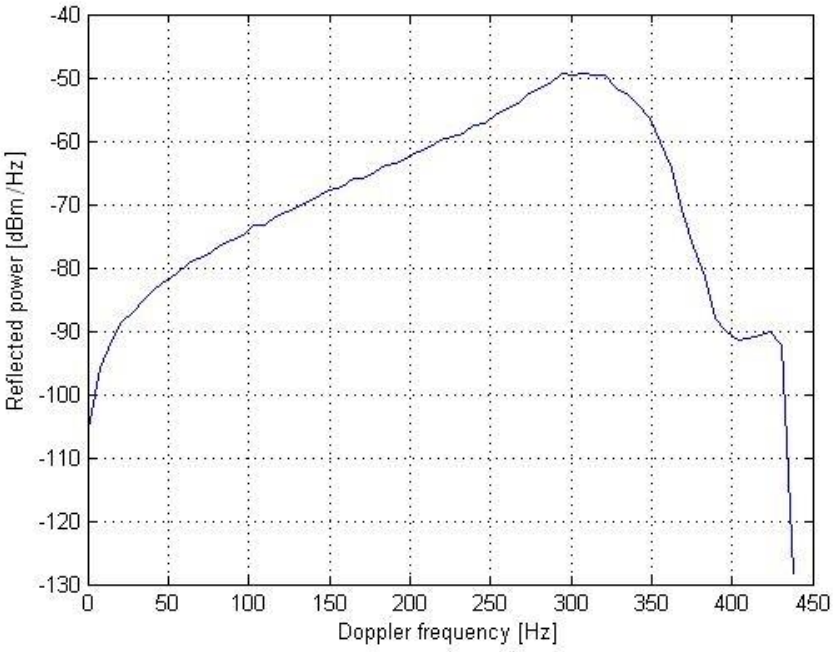


*Figure 17 - 256*256 grids*

These three figures clearly show that the resolution of the estimated power spectrum is improving when there are more grids, and the peak value appears when the Doppler frequency is around 300 Hz. According to Equation (2.5), the Doppler frequency when the velocity is 10 km/h should be:

$$f_d = \frac{2vcos\alpha}{c} f_0 = \frac{2 \times 10km/h \times \cos(45°)}{3.0 \times 10^8} \times 24 \times 10^9 = 314.27Hz$$

The calculation result shows that this model is suitable, and it can be developed in the later simulations and computations. The sensitivity of the radar module shown in the datasheet is -76 dBm. In this simulation, the reflected power top value approach is -50 dBm, which means that the reflected power can be detected.

The following two simulation figures display the spectrum when the velocity is 50 km/h and 100 km/h, respectively. Comparing Figures 15 to 17, it is obvious that the spectrum's shape stays the same but spreads widely when the vehicle is accelerated.

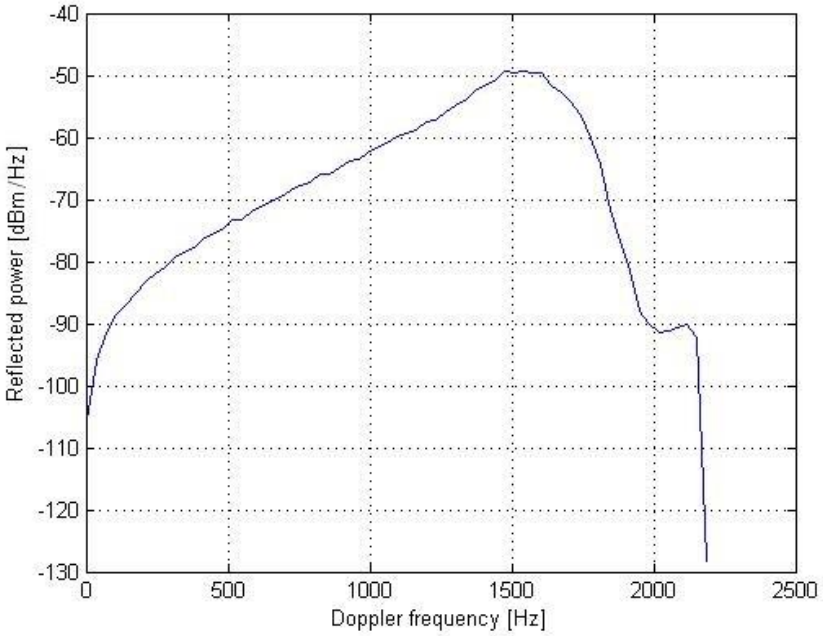


*Figure 18 - Spectrum for v = 50 km/h*

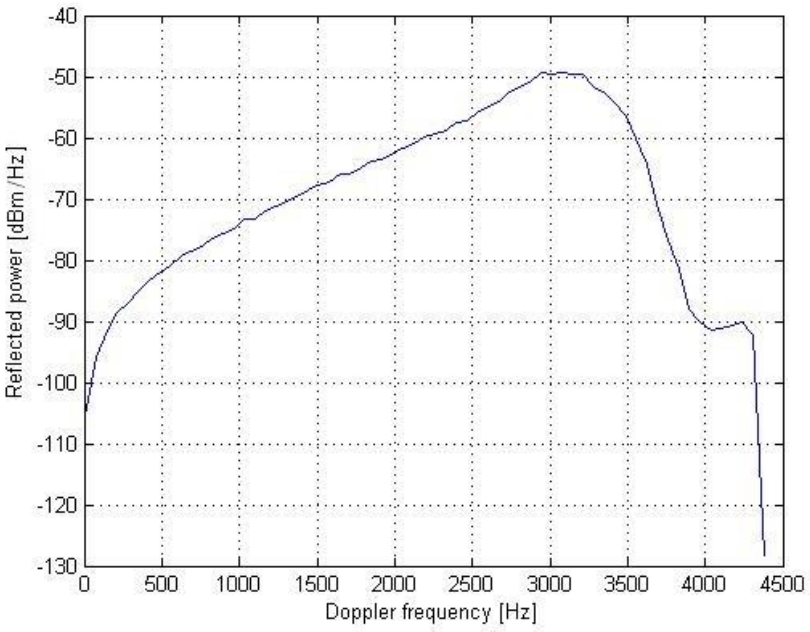


*Figure 19 - Spectrum for v = 100 km/h*

## 3.3 Estimate the received radar signal equation

The radar signal has be expressed in equation (2.6):

$$x(t) = Ae^{i(2\pi f_d t + \theta)}$$

The amplitude of the signal is proportional to the root of the power of the signal. The amplitude A can be replaced by $\sqrt{P_r}$ in Equation (3.2) because the reflected power of each grid has been found in the previous calculations.

$f_d$ in this equation stands for the Doppler frequency from each grid. Angle $\theta$ is the phase. The Doppler frequency does not depend on the phase angle, so that the angle $\theta$ can be a random value. Summing all the values from each grid, the received signal equation is:

$$x(t) = \sum_{n=1}^{Grid\_no} \sqrt{P_r}_n e^{i(2\pi f_{d_n} + \theta)} \qquad (3.3)$$

The received signal is shown below in Figure 20 by running the simulation code in Matlab. The velocity at this moment is 10 km/h.

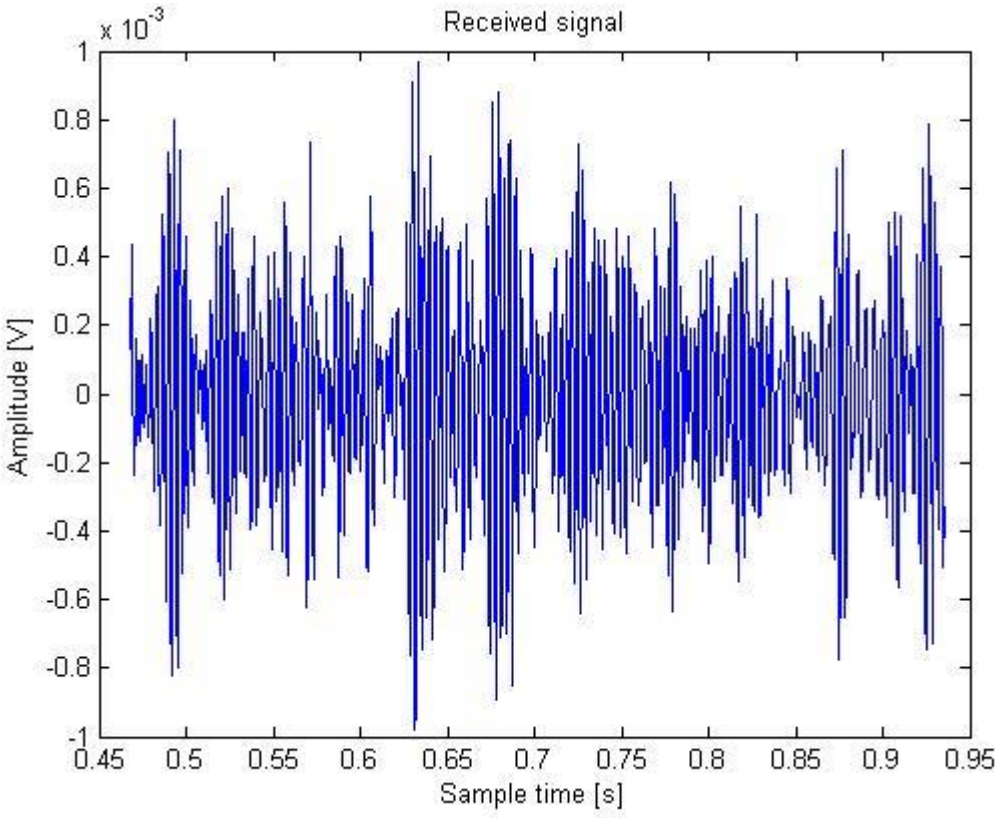


*Figure 20 - Estimated received signal*

# 4. Simulations and analysis

In the previous chapters, the equation of the received signal was found and the frequently used algorithms were introduced. This chapter performs the simulations based on the data which have already been calculated. From these simulations, a proper algorithm is determined for the system.

## 4.1 Simulations without noise

The received Doppler signal expression was presented in Chapter 3, Equation (3.3):

$$x(t) = \sum_{n=1}^{Grid\_no} \sqrt{P_r}_n e^{i(2\pi f_{dn}+\theta)}$$

It should be noticed that the radar signal here is an ideal signal without any noise. The signal with noise will be analyzed later if the spectrum of the signal without noise can be worked out successfully.

### 4.1.1 Simulations based on classical methods

In the first simulation, the four classical methods presented previously are compared. They are the periodogram, the Bartlett method, the Welch method and the BT method. The range of the expected Doppler frequency value can be estimated approximately with Equation (2.5). Take the velocity of 1 m/s as an example:

$$f_d = \frac{2vcos\alpha}{c} f_0$$

In this case the Doppler frequency is not greater than 120 Hz. According to the Nyquist-Shannon sampling theorem, the sampling frequency should be at least twice the Doppler frequency. In the Matlab code, the sampling frequency is set at five times the maximum Doppler frequency. The sample point in FFT computation is set to NFFT=1024. The Doppler frequency is:

$$f_d = \frac{2vcos\alpha}{c} f_0 = \frac{2 \times 1m/s \times \cos(45°)}{3.0 \times 10^8 m/s} \times 24 \times 10^9 \text{Hz} = 113Hz$$

This means that there should be a peak at the point where the frequency is 113 Hz in the power spectrum. The simulation result is shown below in Figure 21. The same window, the rectangular window, is used in the four methods. The figure illustrates that all four methods show a peak at around 100 Hz, and the Welch method shows the best performance among the four methods.

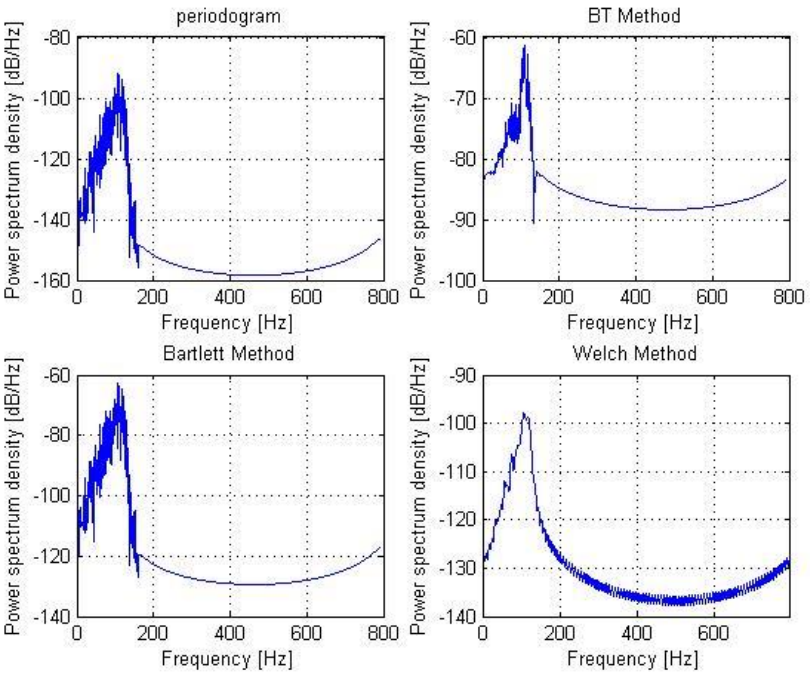


*Figure 21 - Classical methods for PSD estimation*

It should be remarked here that the theoretical signal is a complex signal, and the spectrum should be symmetric about the axis where the frequency is equal to zero Hz, but I did not discover how to change the display format in Matlab.

The following simulations illustrate the comparison of the five window functions, which were introduced in Chapter 2. The simulations are based on the Welch method, because it has the best performance in the previous simulation. The result is displayed below in Figure 22.

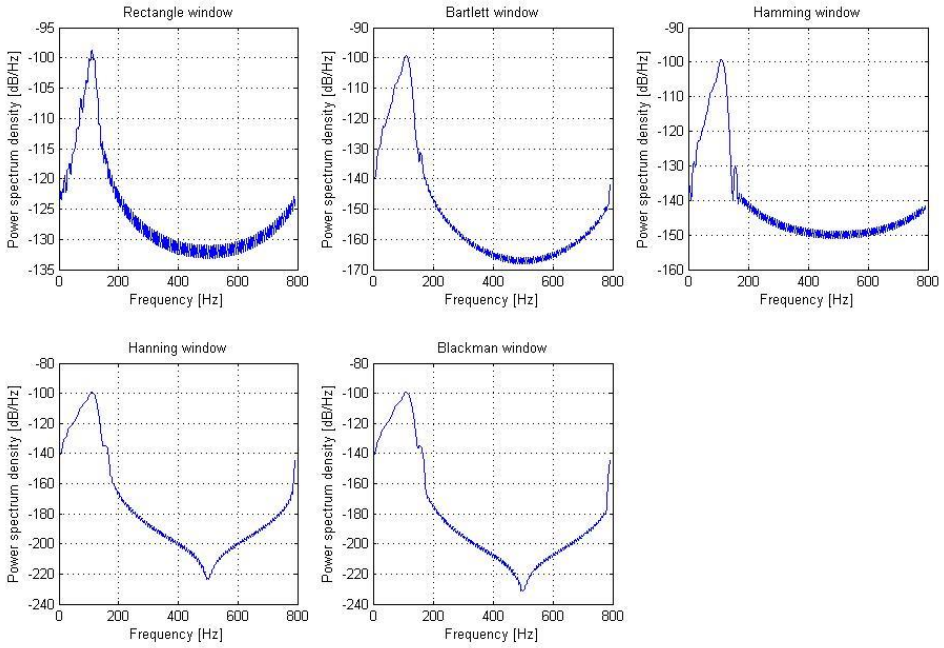


*Figure 22 - Welch methods with different windows*

As the figures show, the spectrum filtered by the rectangular window has the narrowest band. The differences between the rectangular window, the Bartlett window and the Hamming window are relatively small. The effect of the Hanning window is similar to that of the Blackman window. To select a proper window function, it is necessary to consider the properties of the analyzed signal and what is requested of our system. The request here is to pick out the peak value and the relevant Doppler frequency in the spectrum, and obviously all the above windows meet the request. In this thesis, the simplest window, the rectangular window, can be selected [28].

### 4.1.2 Simulations based on AR model

The three popular methods of the AR model were introduced in the previous section. All three methods have both advantages and disadvantages, and it is difficult to decide which one is the best for this system. To make a further comparison of the three methods, some simulations are run in this section.

In the first simulations, the received radar signal is the ideal theoretical signal without any noise. The white noise is added in the second simulations if the three methods have a satisfactory performance in the first simulations.

The resolution of the geometric model is set to 128×128 grids. Too high a resolution in the geometric model will cause a long run time in Matlab. Suppose the velocity is equal to 1 m/s. As previously calculated, the expected Doppler frequency should be shown at 113 Hz. The simulations' results are listed below:

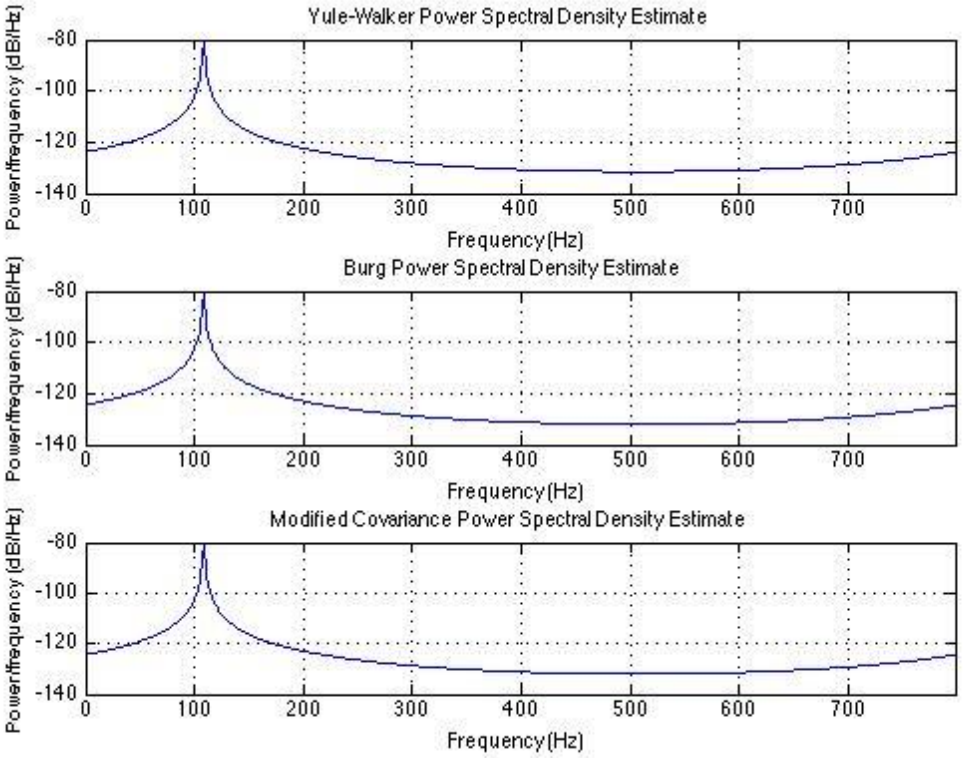


*Figure 23 - AR model with order =1*

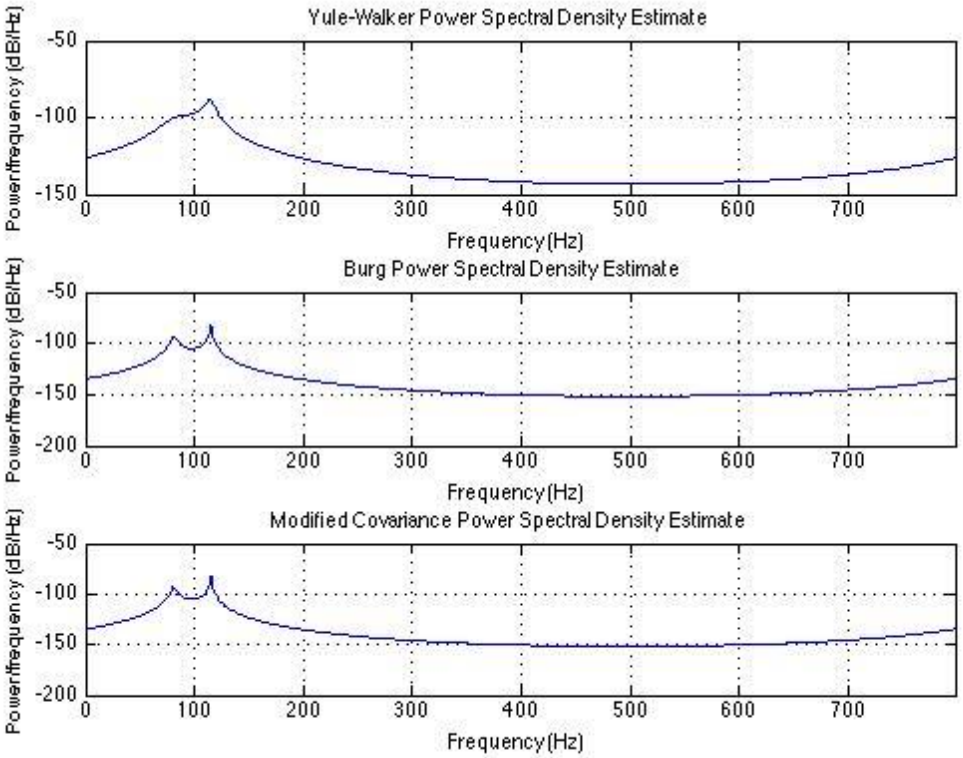


*Figure 24 - AR model with order =2*

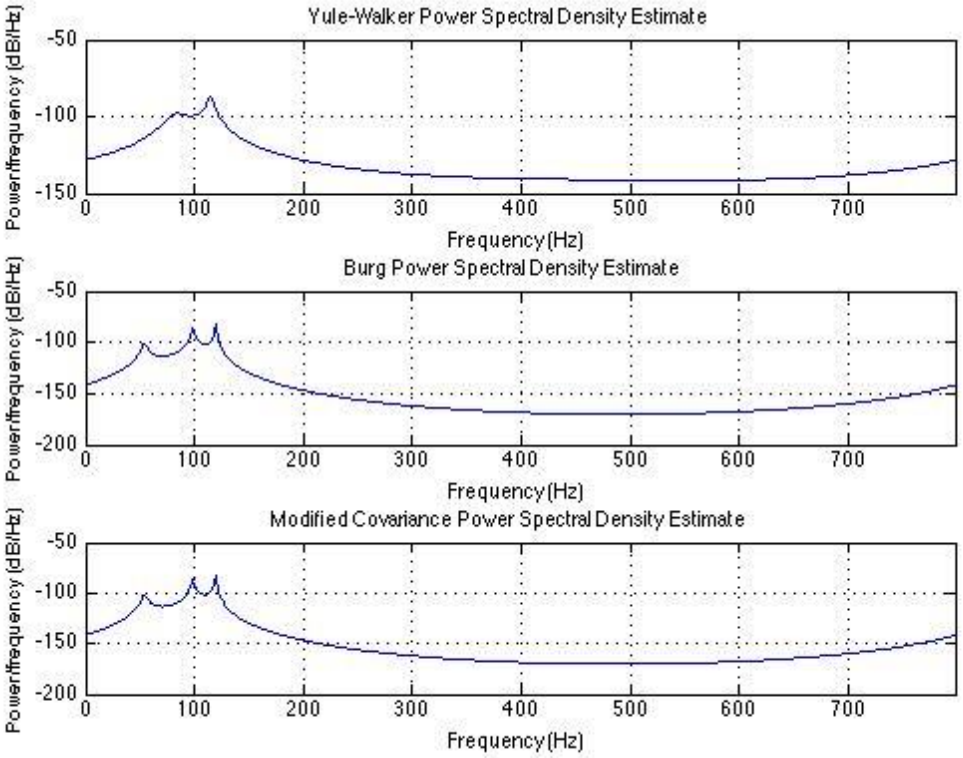


*Figure 25 - AR model with order =3*

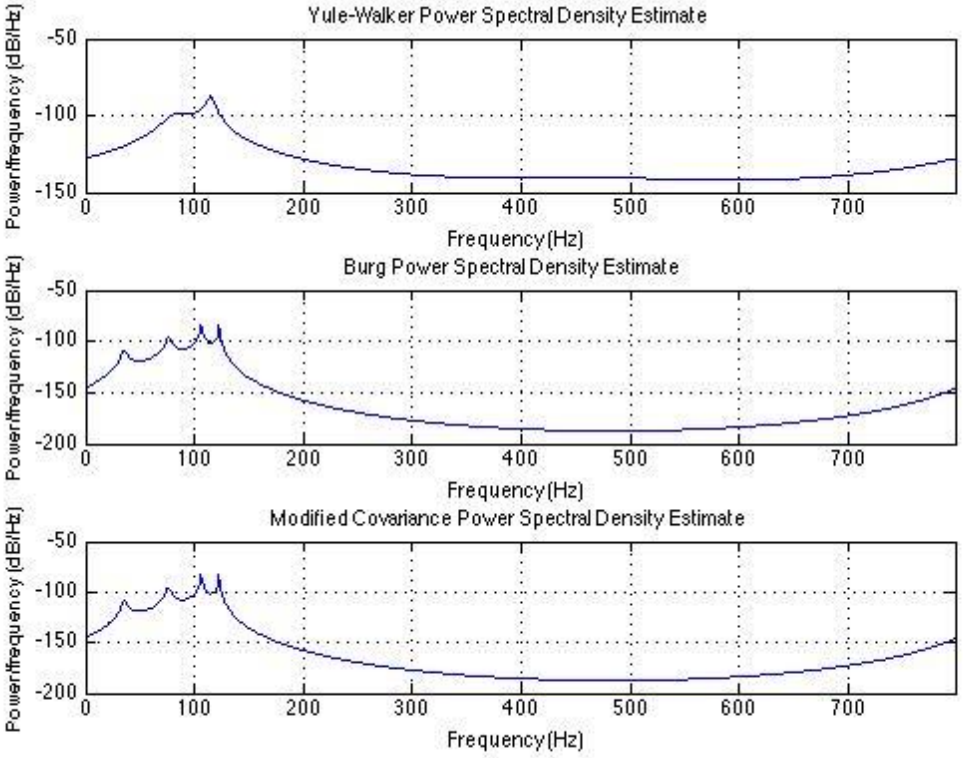


*Figure 26 - AR model with order =4*

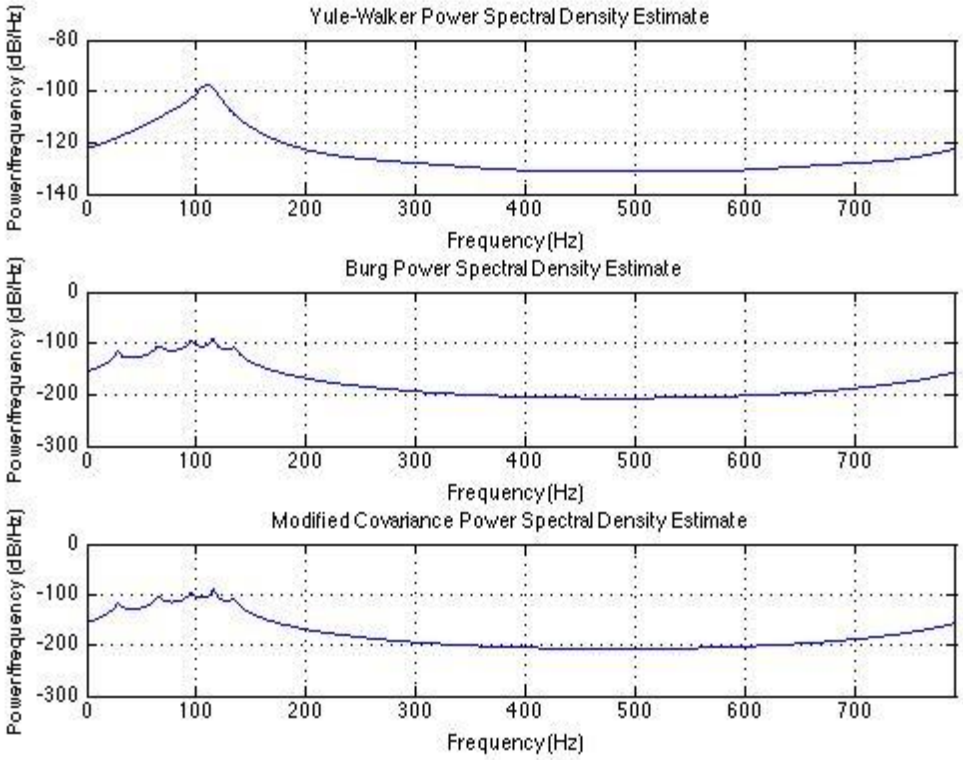


*Figure 27 - AR model with order =5*

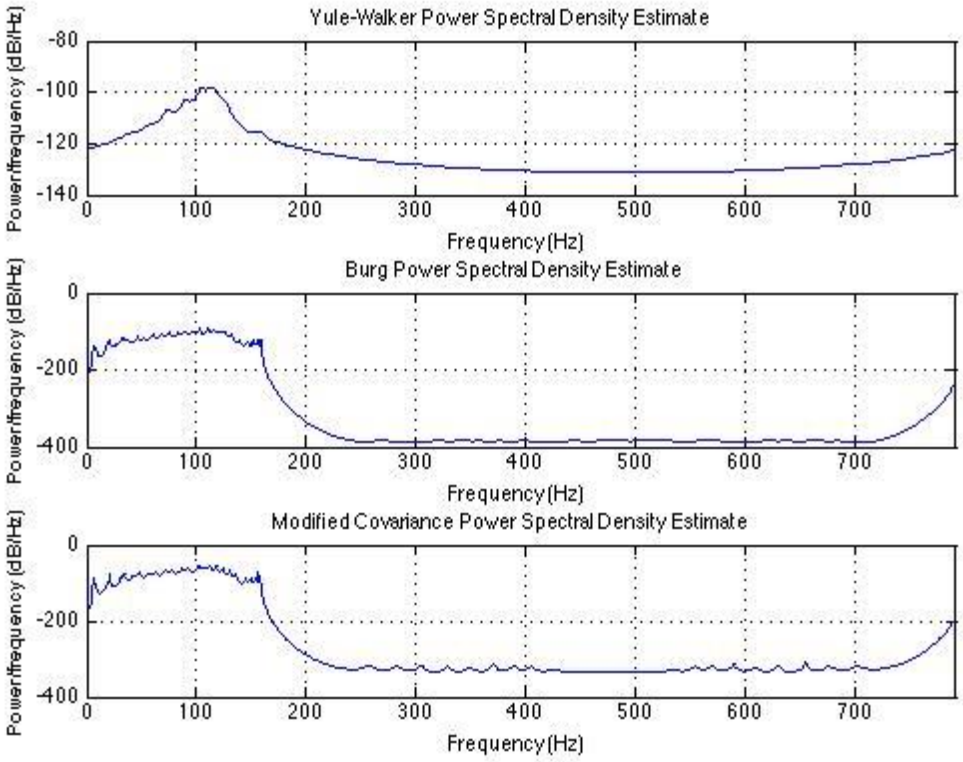


*Figure 28 - AR model with order =50*

Without the noise, the Yule-walker method gives the best result. The peak value can easily be read from the power spectrum. With different orders in the calculations, the performances are different. In Figure 21, the order of these three methods is set to one, and there is no difference between them. When the order increases, the spectra of the Burg method and the Marple method begin to show more than one peak, and the number of peaks is the same as the order number. It is difficult to find the valid Doppler frequency corresponding to the current velocity. Generally speaking, the greater the order is, the more precise the result is, but too great an order will increase the variance and the computation time. The target in this thesis is to find out the Doppler frequency, so that any of the three methods can be selected when the order is set to one, and the limitation is that there is no noise in the signal.

## 4.2 Simulation with noise

In the second simulations, the Gaussian white noise is appended and the signal noise ratios (SNR) are set respectively to 1dB, -10 dB, -15 dB and -20 dB. To observe how the SNR affect these three methods, the solution is to hold the order constant as one, and only one, SNR varies.

### 4.2.1 Simulations based on classical methods

The following simulations reveal how the classical methods work with the signal with Gaussian white noise. The figures below display the spectra of the received Doppler signal with noise.

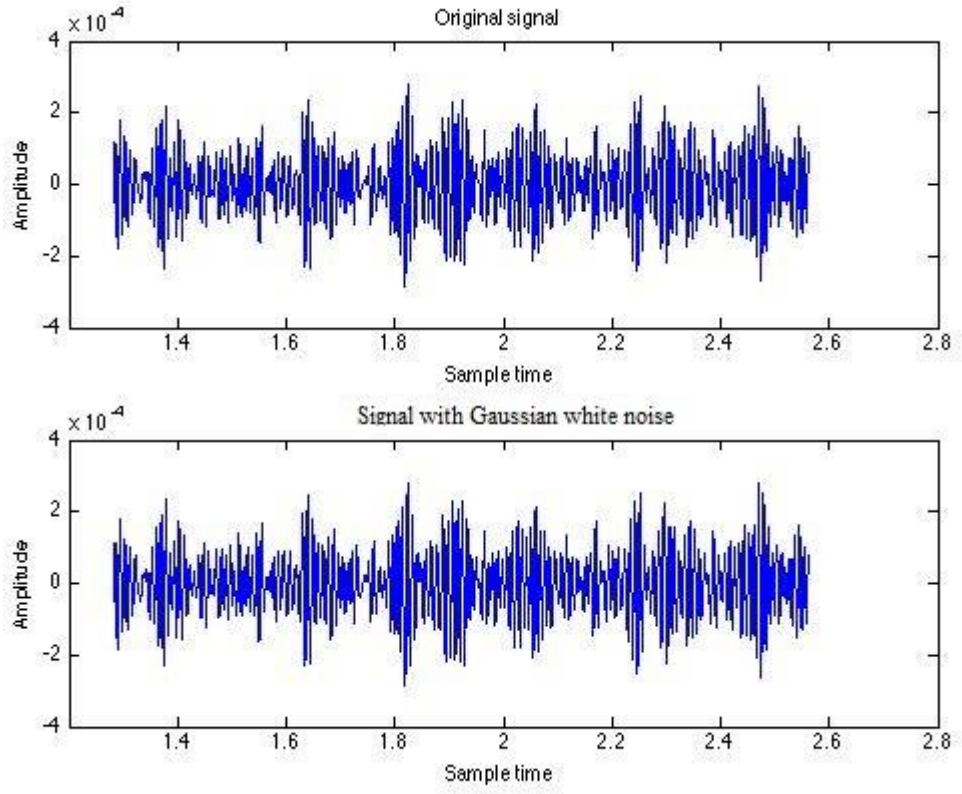


*Figure 29 - Signal with white noise with SNR = 1dB*

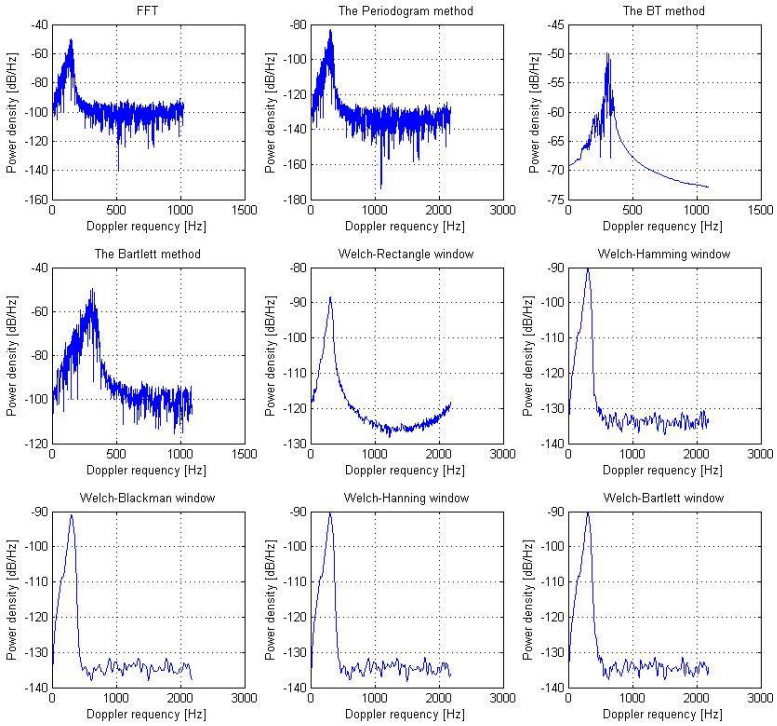


*Figure 30 - Classical PSD methods for signal with SNR =1dB*

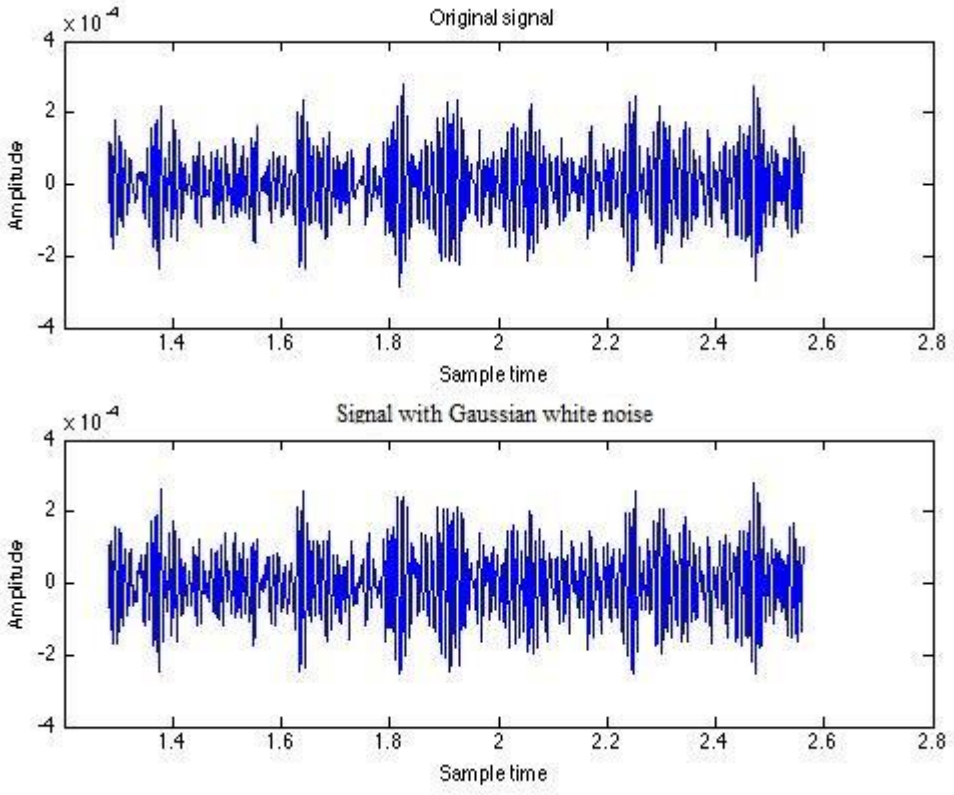


*Figure 31 - Signal with white noise with SNR = -10 dB*

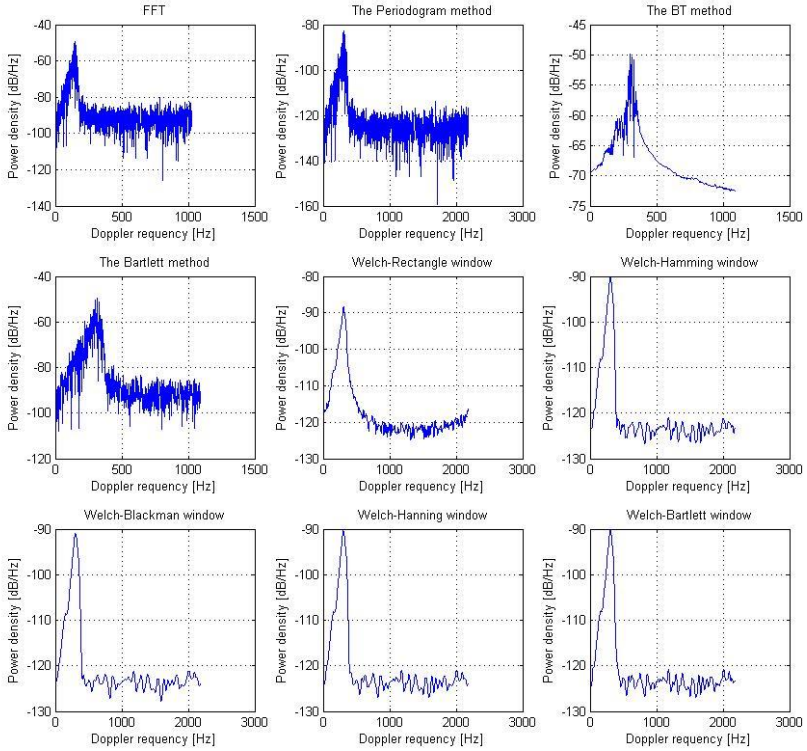


*Figure 32 - Classical PSD methods for signal with SNR = -10*

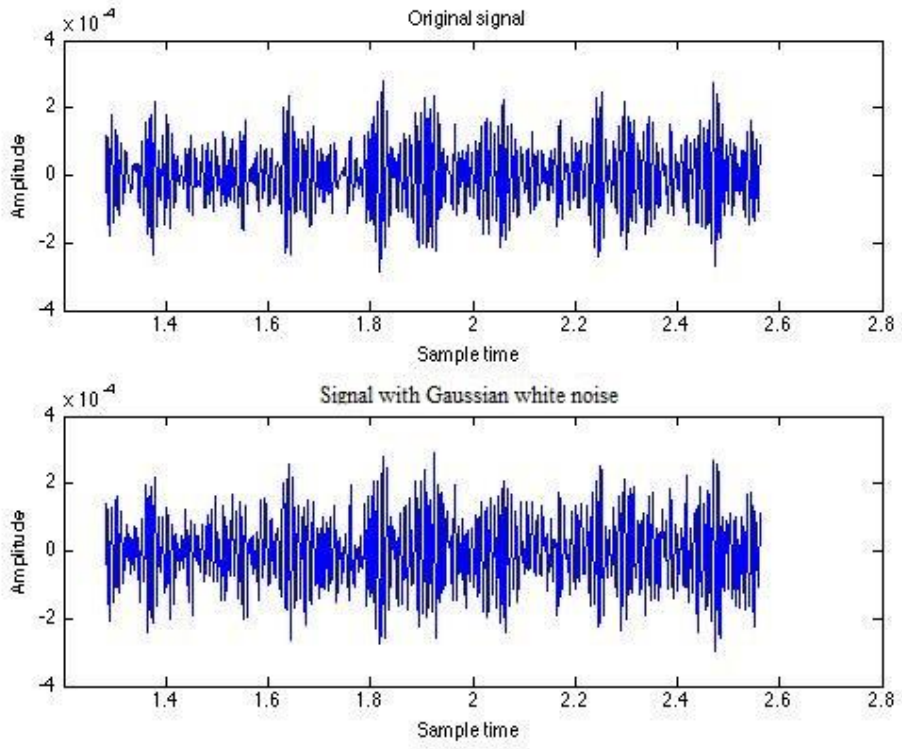


*Figure 33 - Signal with white noise with SNR = -15 dB*

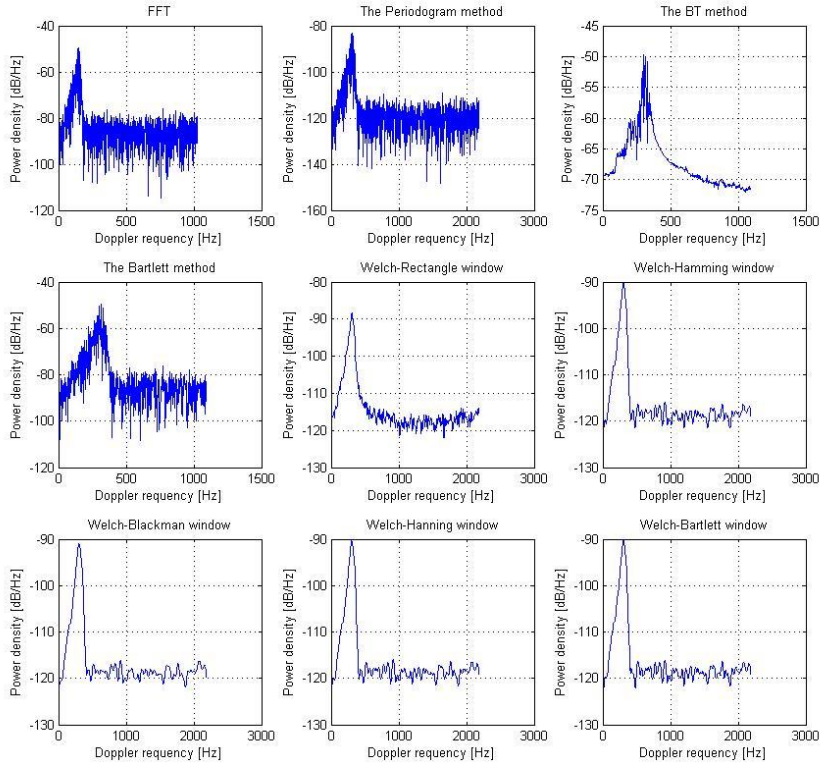


*Figure 34 - Classical PSD methods for signal with SNR = -15 dB*

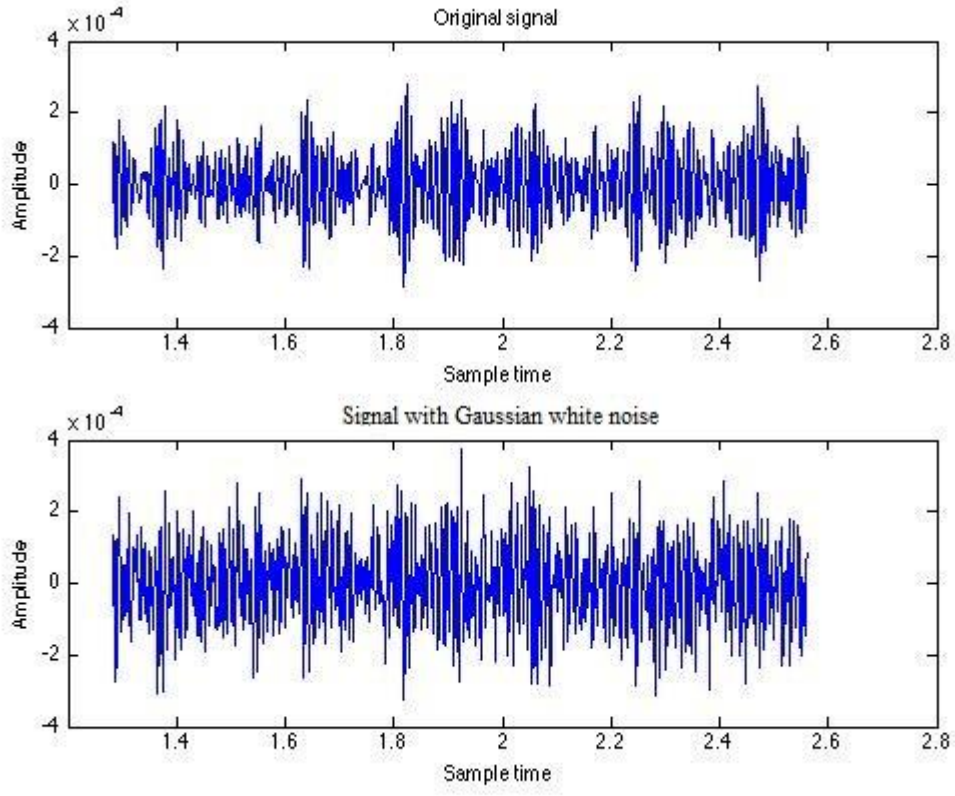


*Figure 35 - Signal with white noise with SNR = -20 dB*

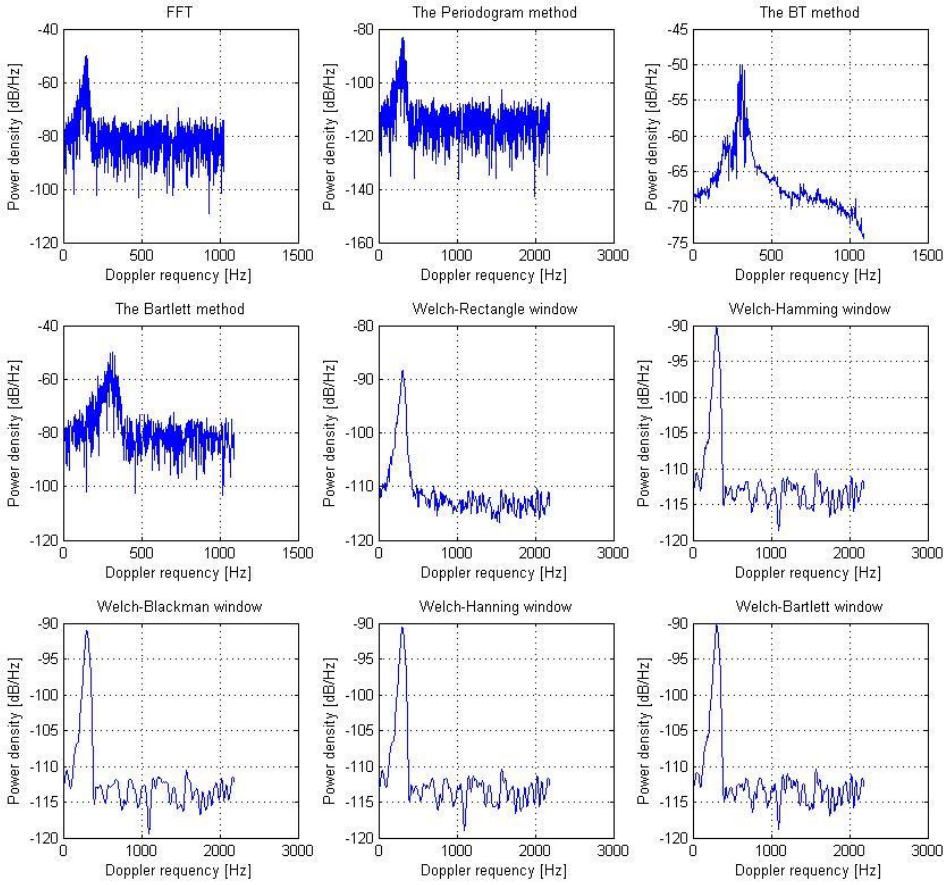


*Figure 36 - Classical PSD methods for signal with SNR = -20*

The figures show that the resolutions of the classical methods are getting worse and worse when the SNR increases, especially for the direct FFT method, the periodogram method, the BT method and the Bartlett method. It is not possible to read the peak value from the spectra based on these four methods. The performances of the Welch method with different window functions are relatively better with respect to the other four methods.

### 4.2.2 Simulations based on AR model

The next simulations show the performances of the three methods based on the AR model.

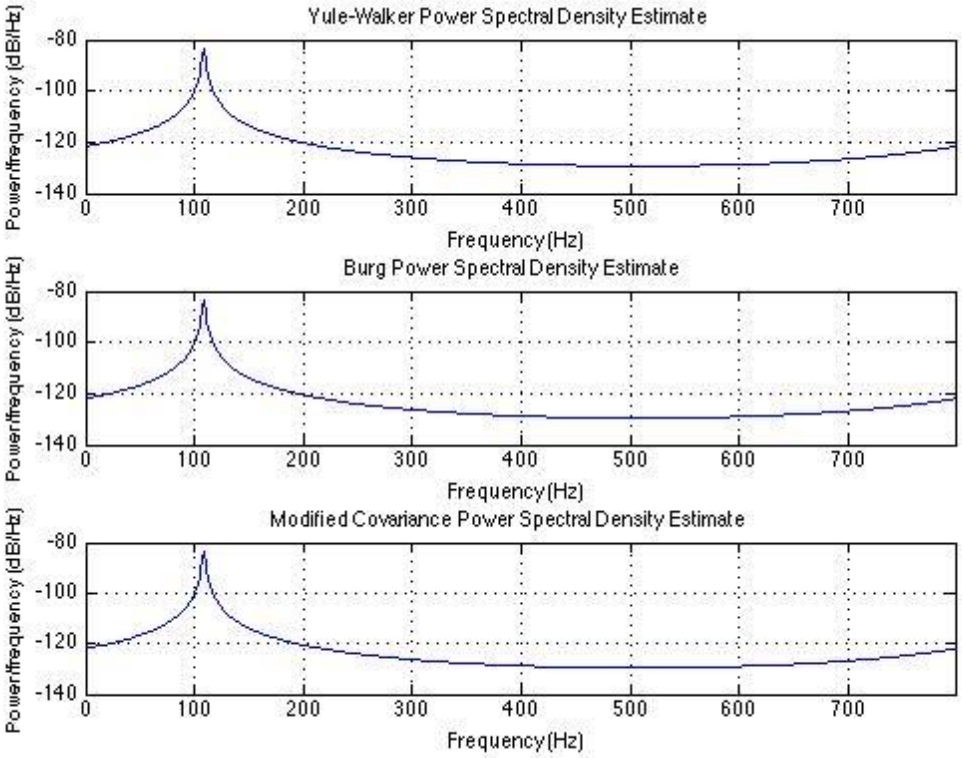


*Figure 37 - AR method for signal with SNR = 1 dB*

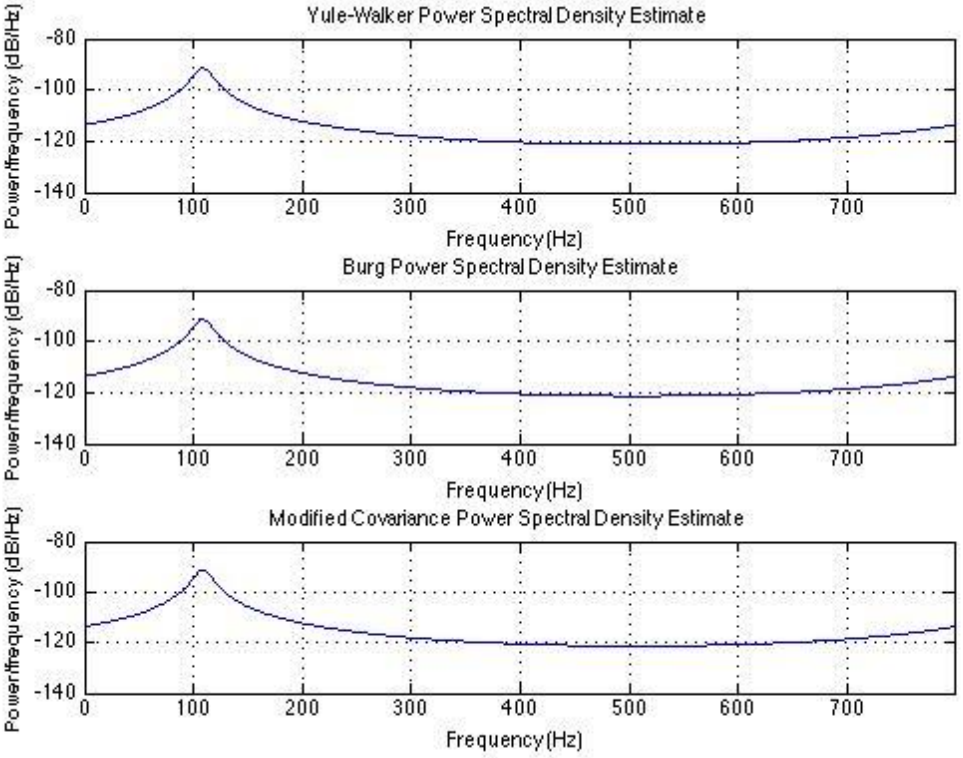


*Figure 38 - AR method for signal with SNR = -10 dB*

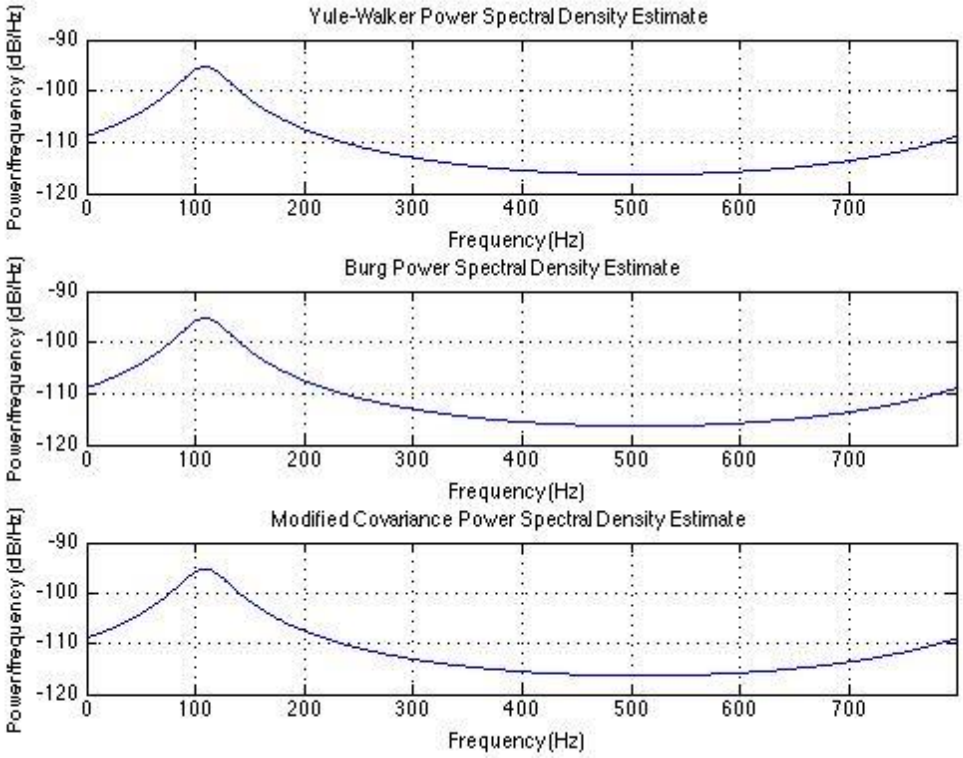


*Figure 39 - AR method for signal with SNR = -15 dB*

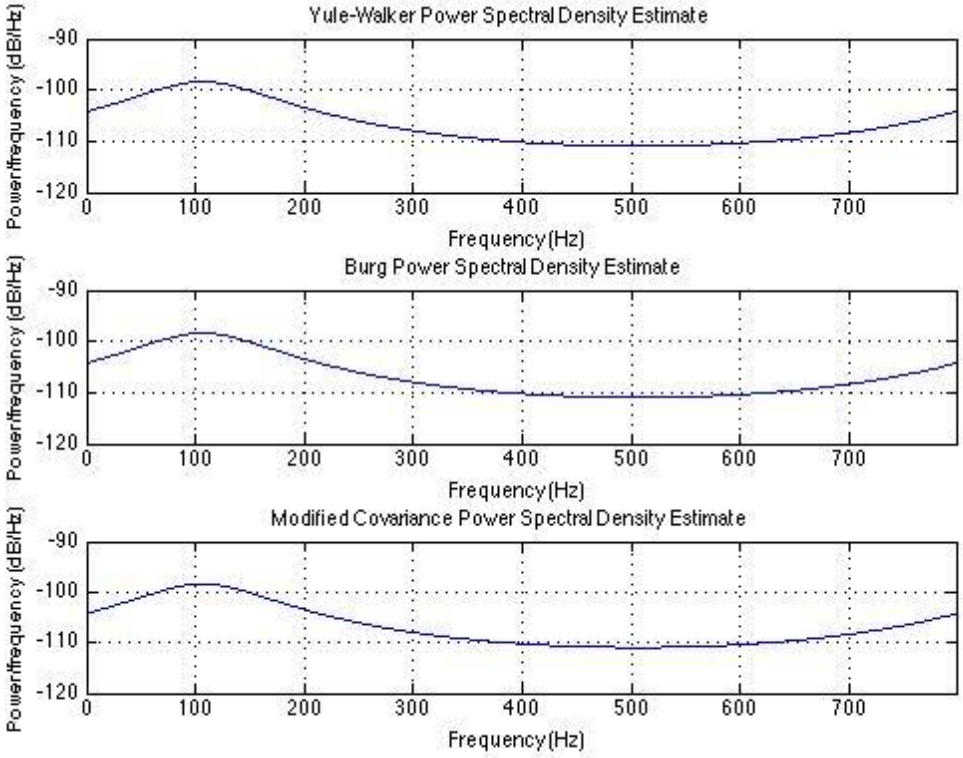


*Figure 40 - AR method for signal with SNR = -20 dB*

The noise level increases from 1 dB to -20 dB during the simulations. All three methods have the ability to handle the signal accompanied with noise up to -20 dB. This means that the three algorithms work properly, even when the power of the noise is 300 times stronger than the power of the signals.

Now hold the SNR constant as -15 dB and change the orders. The simulations illustrate how the three methods perform with different orders when the noise is added.

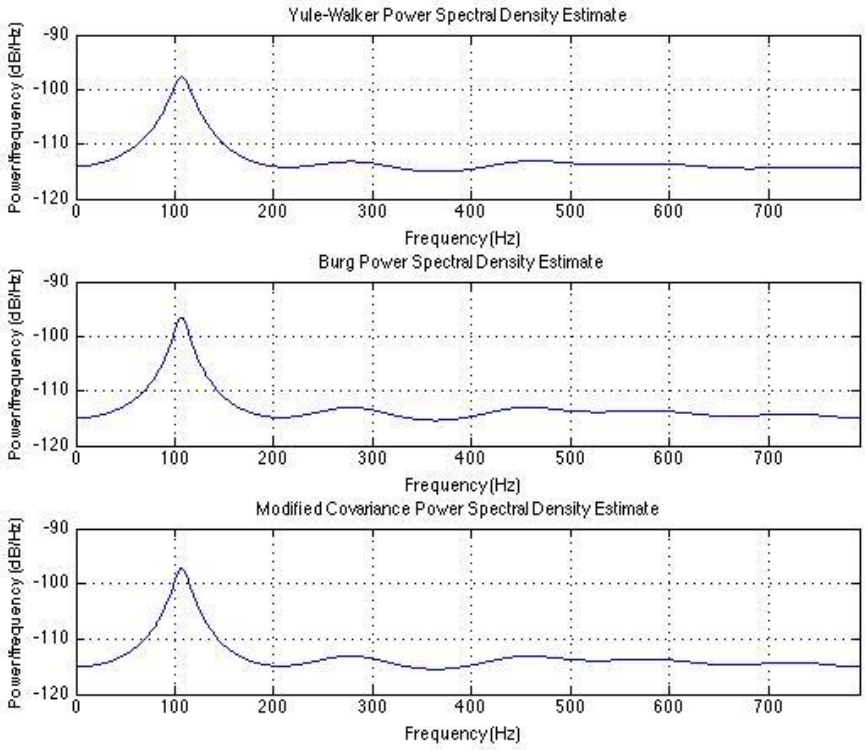


*Figure 41 - AR model with order = 5*

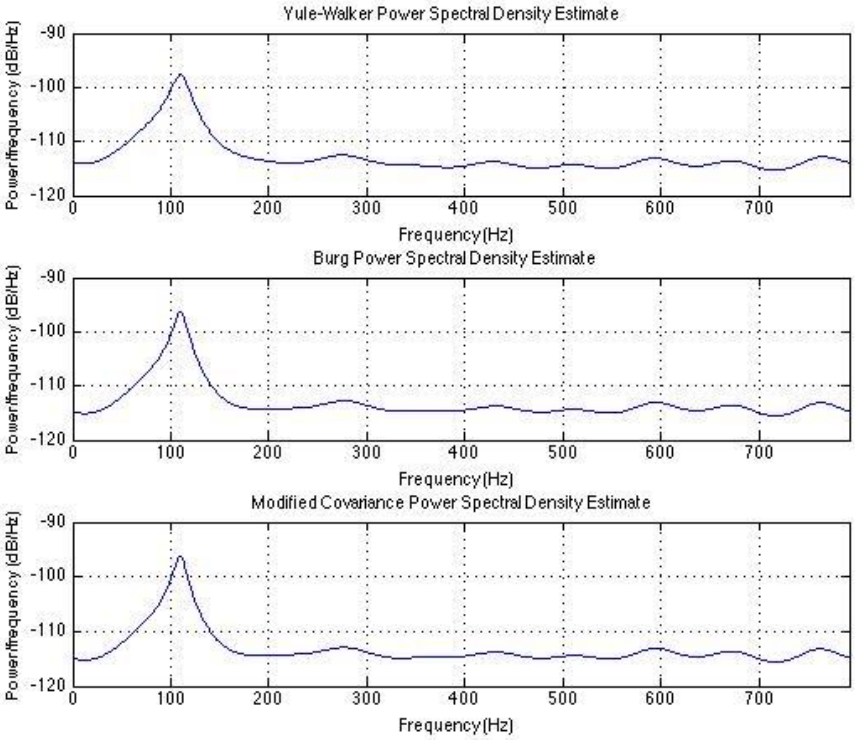


*Figure 42 - AR model with order = 10*

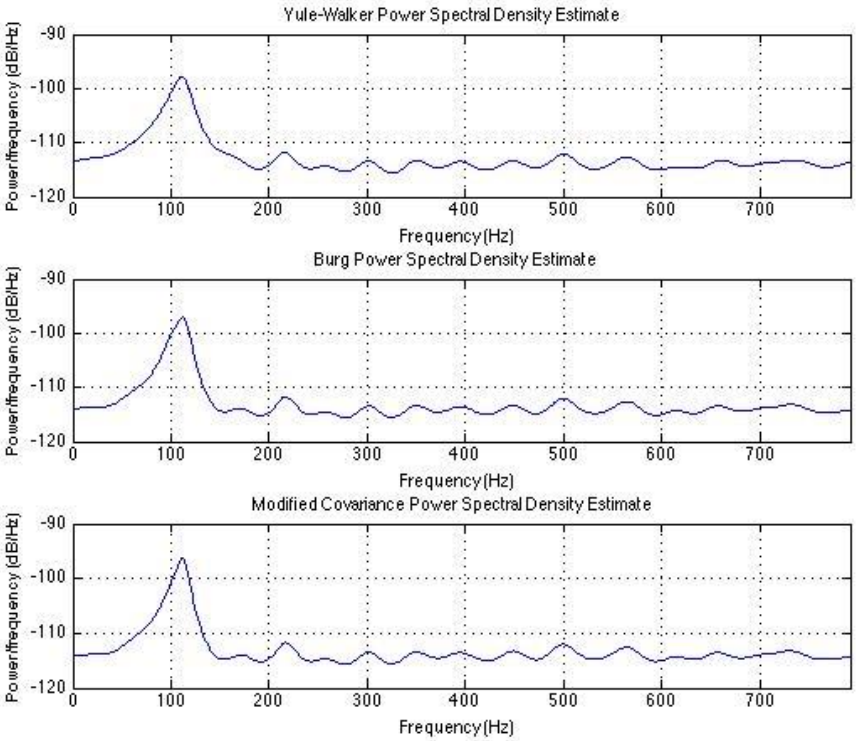


*Figure 43 - AR model with order = 20*

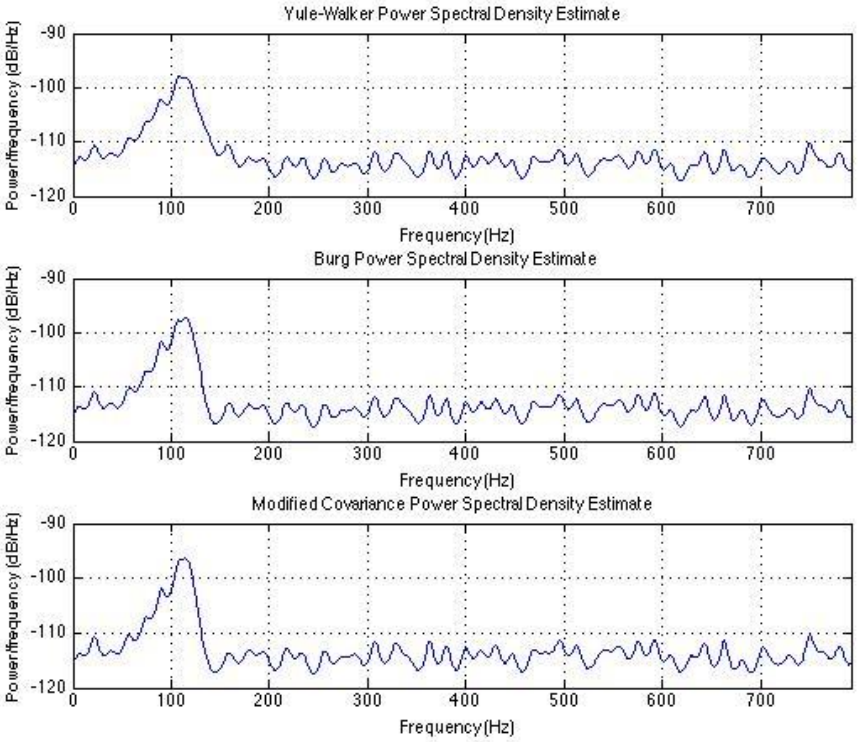


*Figure 44 - AR model with order = 50*

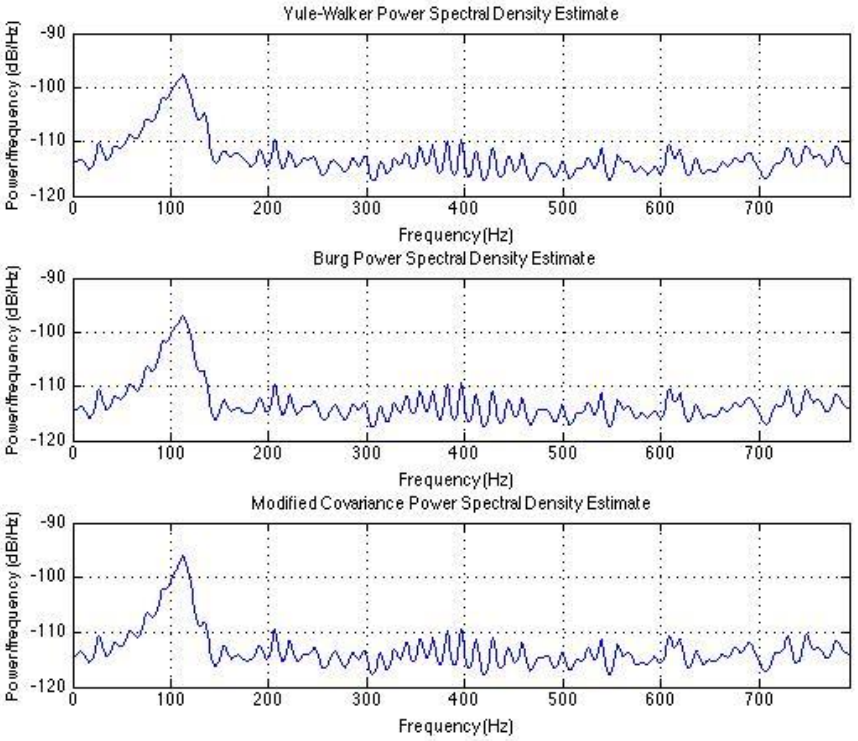


*Figure 45 - AR model with order = 60*

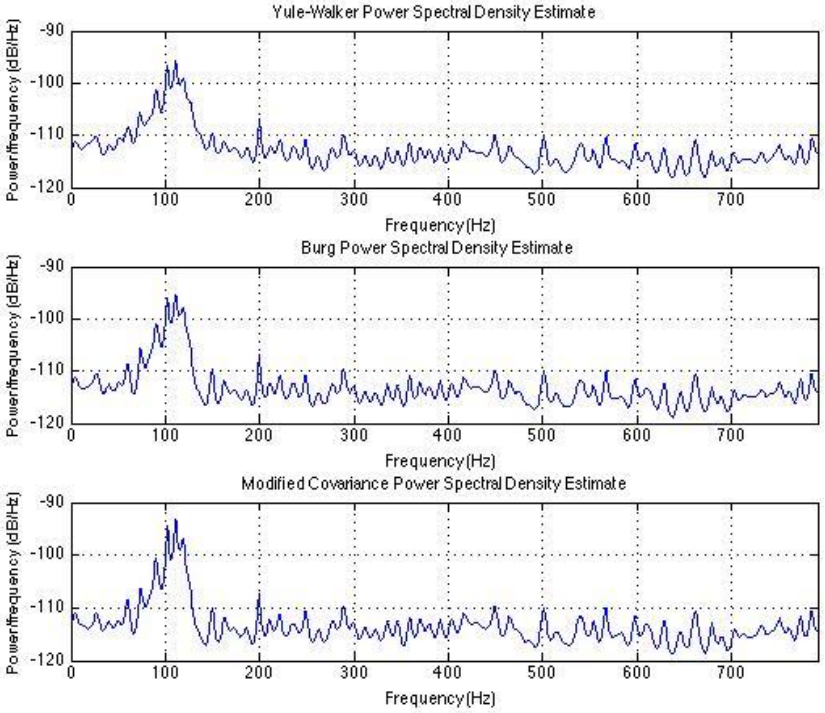


*Figure 46 - AR model with order = 80*

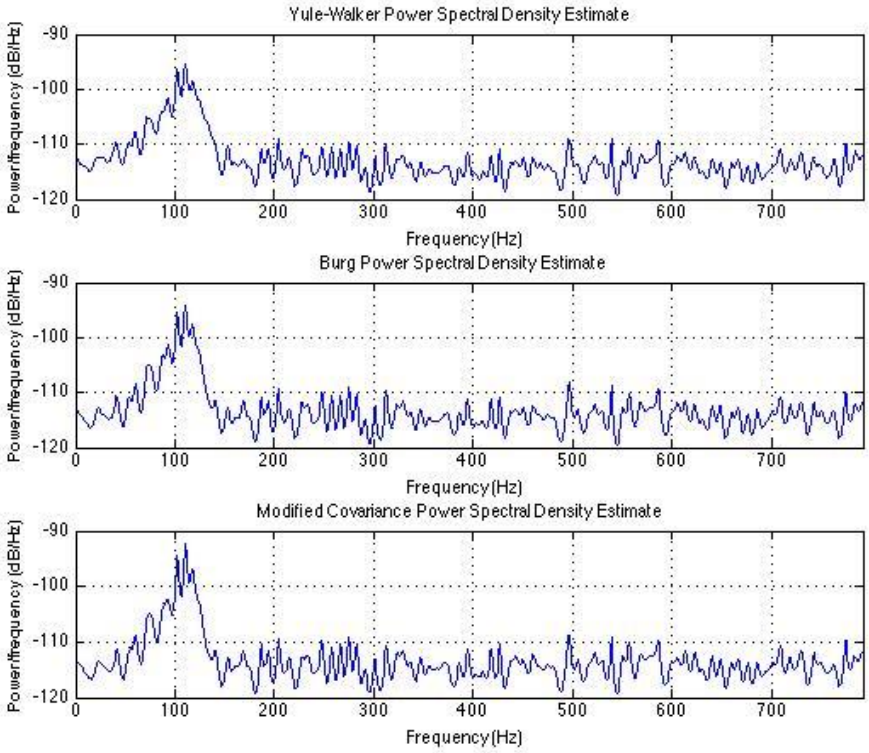


*Figure 47 - AR model with order = 100*

The simulation results show that the variance increases with the increasing order. Although the higher the order, the better the resolution is, more peaks appear in Figure 44 in the spectrum when the order increases. This does not mean that the greater the order, the better the result is. The only information this thesis cares about in the spectrum is the peak value. The other information shown in the spectrum makes no difference. To avoid the needless computations, the order should be set as low as possible.

In these simulations we use the method in which only one factor changes at one time, SNR or order. By comparing the simulation results, it is not difficult to find out how each factor affects the performance of these three methods.

Generally speaking the three methods based on the AR model can result in a better power spectrum estimation than the classical methods. The Welch methods with window functions are better than the other classical methods. Although the other methods such as direct FFT, the periodogram, the BT method and the Bartlett do not perform as well as the modern PSD estimation methods, they are simple to understand and implement, and so they are widely used. In this system, the AR model is selected to estimate the spectrum.

# 5. Measurements and results

All the theory background and calculations have been covered in the previous chapters. The measurements are taken in this section. The company Q-Free at Trondheim, which arranged this master thesis topic, provided us with a mail van to implement the measurements. This section introduces the equipment employed during the measurements and the measured data.

## 5.1 Equipment

This section introduces the hardware equipment employed in the measurements.

### 5.1.1 Doppler radar module MDU2410

This module was developed by Microwave Solutions Ltd in England. The radar coverage pattern and other relevant information about this module were shown in the previous chapter.

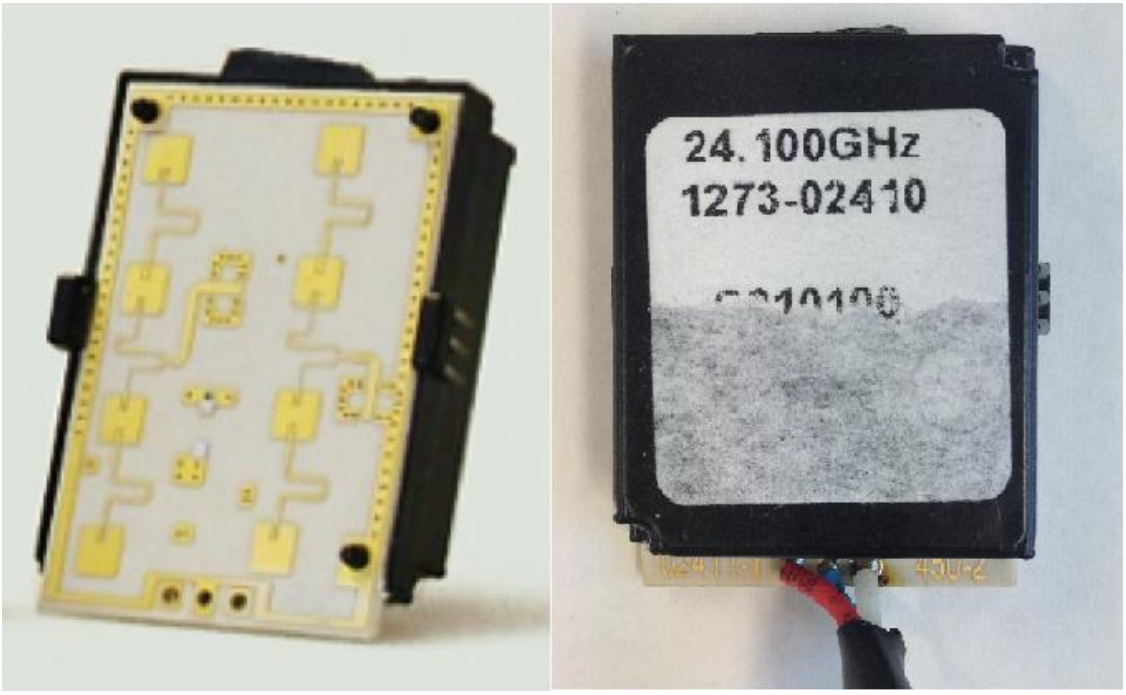


*Figure 48 - Doppler radar module*

The radar circuit description is illustrated below in Figure 49. The radar transmits the signal and receives the reflected signal. There is a mixer, which mixes the transmitted signal and received signal and outputs the Doppler signal.

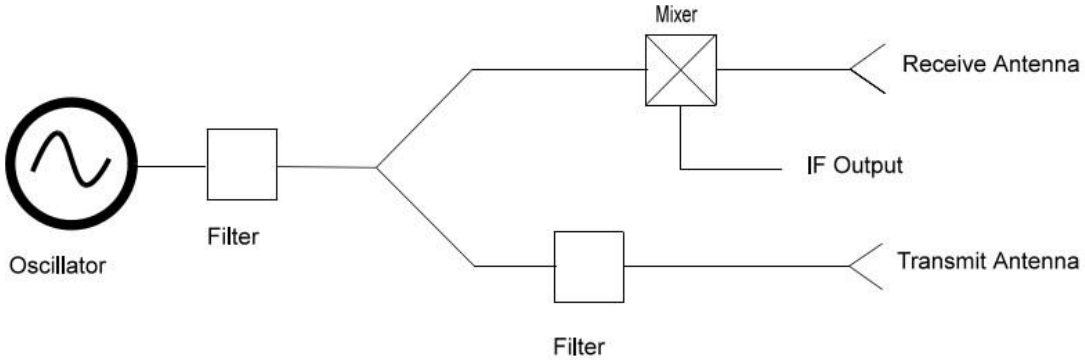


*Figure 49 - Circuit descriptions [9]*

### 5.1.2 Microcontroller MCB4300

The evaluation board MCB4300 developed by Keil is equipped with the ARM cortex-M4 digital signal processor. There is a Secure Digital card (SD card) slot for the SD card to record the measured data. The screen on the board displays the power spectrum and the current velocity in real time. The Doppler signal output from the Doppler radar is an IF signal, which is sampled by the evaluation board from the microphone port. All the software work is done by Joacim Dybedal, who is in charge of all the software tasks in the same master thesis topic.

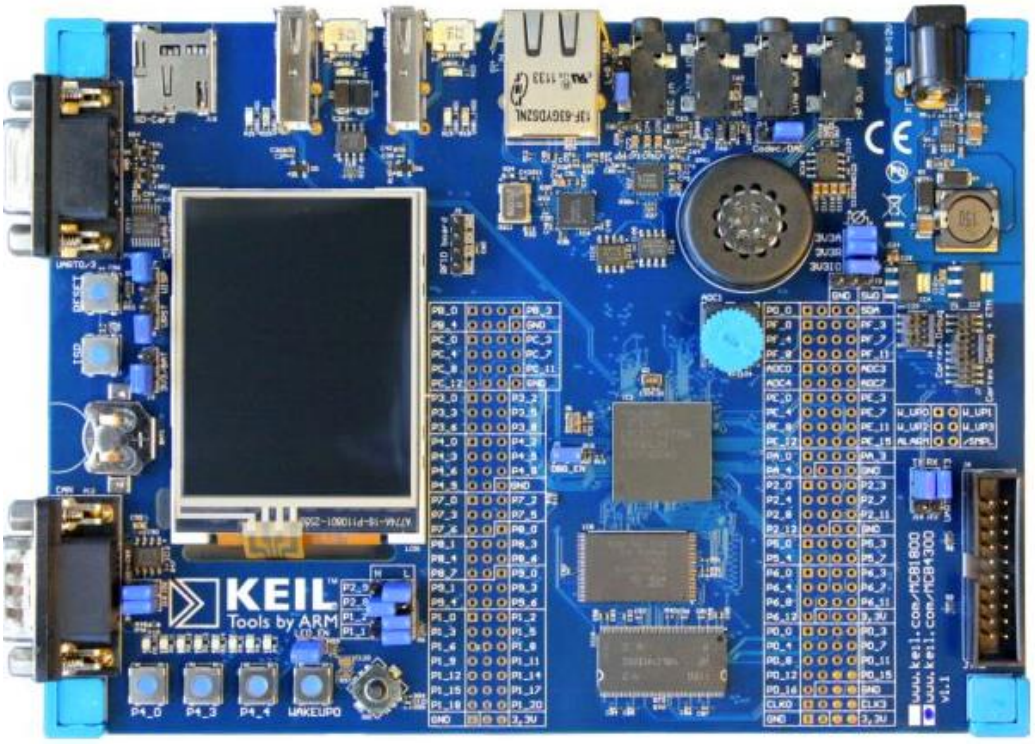


*Figure 50 - Microcontroller MCB4300*

### 5.1.3 Mail van

As previously described, the Doppler radar should be fastened 45-degree face to the road. In consideration of the possibility of the signal being reflected by the bonnet of

the mail van, it is decided to set up the radar behind the car. Figure 51 below shows how the radar was fixed on the back window of the car.

*Figure 51 – Radar mounted on the window*

Figure 52 shows the Doppler radar on the bumper of the car. In this situation the Doppler radar receives a much stronger reflected signal than the situation shown in Figure 51 because of the shorter distance to the road. The measurements are implemented in both these situations.

*Figure 52 – Radar mounted on the bumper*

## 5.2 Measurement plan

An easy measurement table is shown in Table 3. The Doppler signal is sampled and saved as WAV form [29] format in the SD card on the evaluation board. The Doppler signal can be extracted with the help of Matlab. Two groups of data are recorded, one with the radar fastened on the window, and one with the radar mounted on the bumper.

*Table 3 - Measurement data*

| File no. | Velocity km/h | Estimated $f_d$ Hz |
|---|---|---|

| | | |
|---|---|---|
| 1 | 20 | 680 |
| 2 | 30 | 1021 |
| 3 | 40 | 1362 |
| 5 | 60 | 2043 |
| 6 | 70 | 2383 |

## 5.3 Simulation results

In the simulation results, which are shown below, the measured signal is different from the theoretical signal. The theoretical signal is a complex signal, while the measured signal is a real signal. The complex signal is symmetric with respect to the axis where the frequency is equal to zero. The real signals, which we measured, show only the positive part of the signal. This may lead to the deviations between the theoretical value and the real measured value.

In Matlab the function "wavread" is used to read the saved signal in wav-file. The five figures from Figure 53 to Figure 57 display both the Doppler signal and the spectrum with the radar on the window.

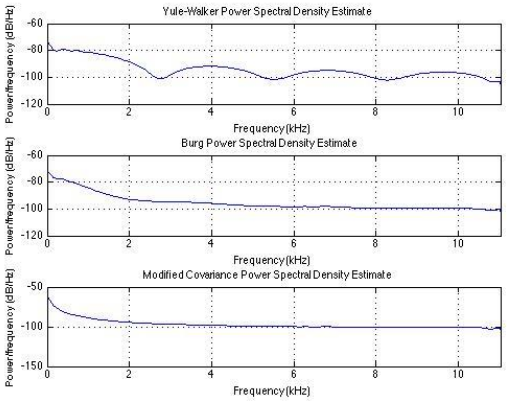


*Figure 53 - Radar on the window at 20 km/h*

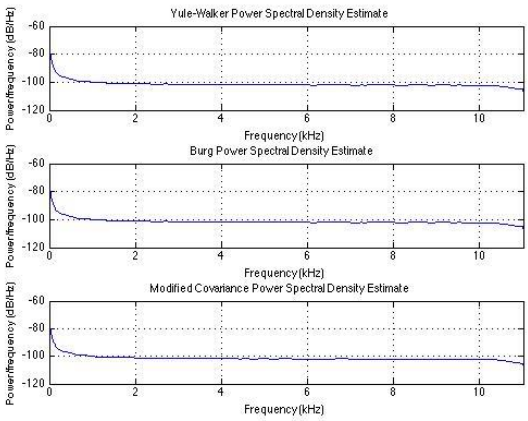


*Figure 54 - Radar on the window at 30 km/h*

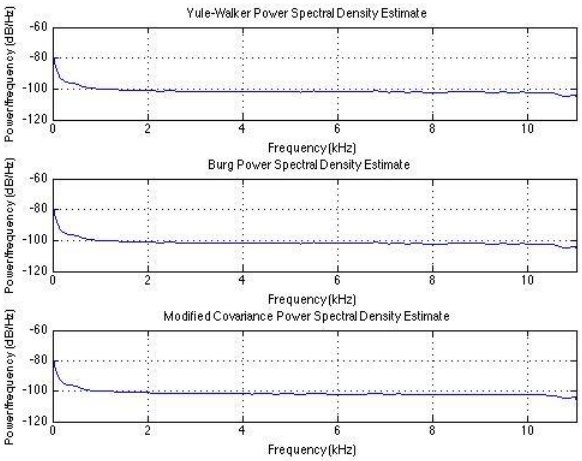


*Figure 55 - Radar on the window at 40 km/h*

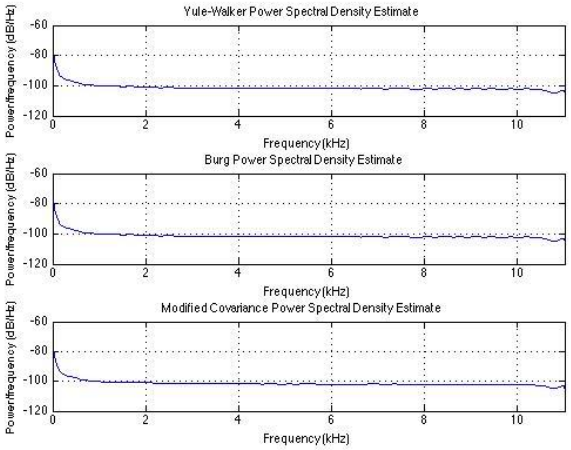


*Figure 56 - Radar on the window at 60 km/h*

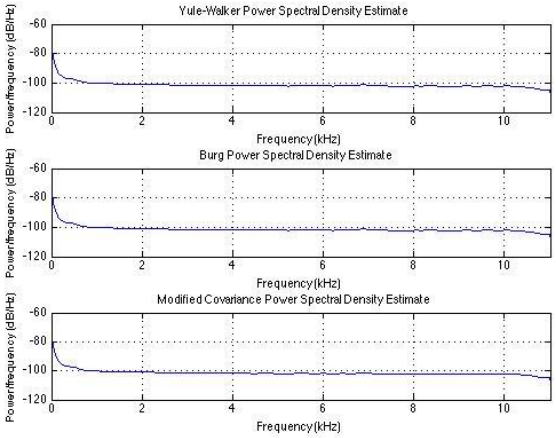


*Figure 57 - Radar on the window at 70 km/h*

It is hard to find out the Doppler frequency in the spectrum. This is because the radar module is mounted on the window and it is 1.5 m from the ground. This does not correspond with the conclusion we reached in Chapter 3. In Chapter 3 it is supposed

that the height of the radar module was 2 m from the ground, and the estimated reflected signal exceeded -70 dB, which means that the reflected signal should be detected when the Doppler radar is set at a height of 2 m. However, the practical measured data show that the Doppler signal cannot be detected when the height of the Doppler radar is even 1.5 m.

The following figures show the spectra of the other group of data measured with the radar fixed on the bumper. This time the height of the radar is 0.5 m.

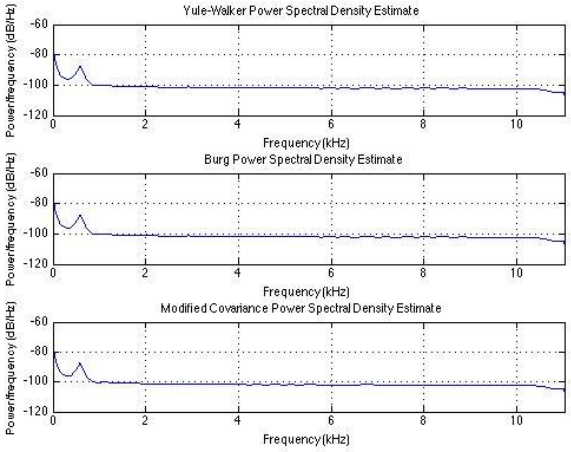


*Figure 58 - Radar on the bumper at 20 km/h*

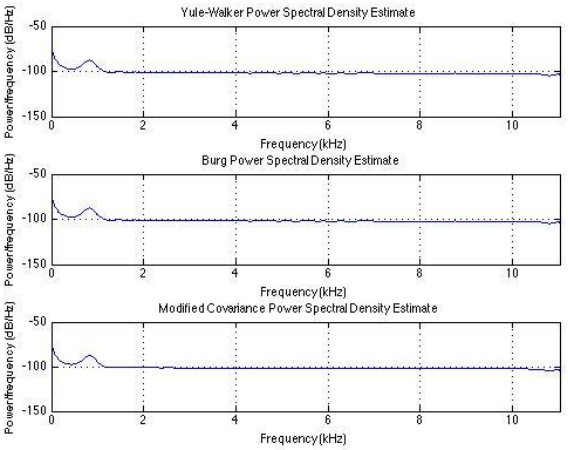


*Figure 59 - Radar on the bumper at 30 km/h*

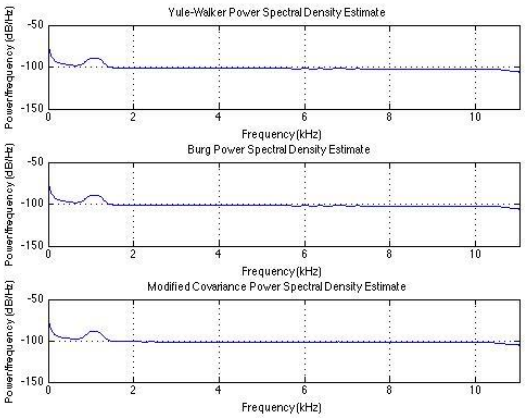


*Figure 60 - Radar on the bumper at 40 km/h*

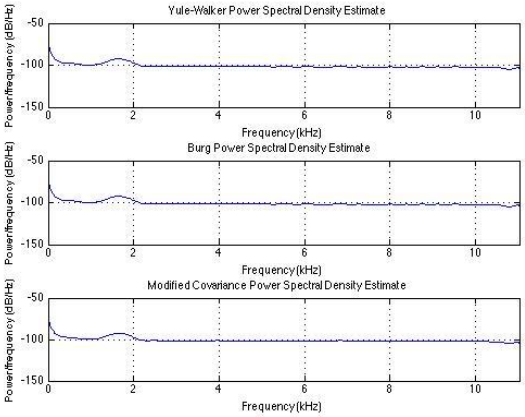


*Figure 61 - Radar on the bumper at 60 km/h*

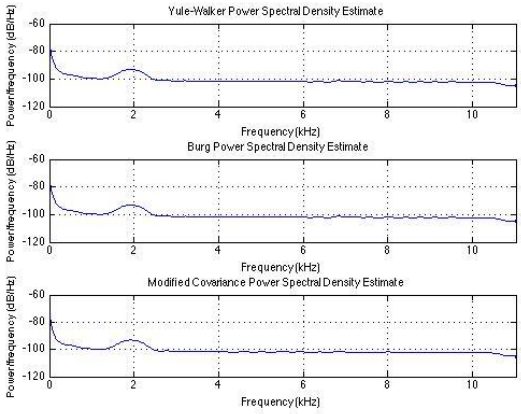


*Figure 62 - Radar on the bumper at 70 km/h*

## 5.4 Results

The spectra of the Doppler signal with different velocities were displayed in the previous chapter. The maximum value is not the Doppler frequency in the spectrum. Observing the spectra, the spectrum begins with a maximum value and then drops significantly within about 200 Hz. This maximum value is caused by some DC components in the evaluations board, which disturbs the peak value in the spectrum. A high pass filter can be adopted here to filter this fault signal. Figure 63 shows the highpass filter.

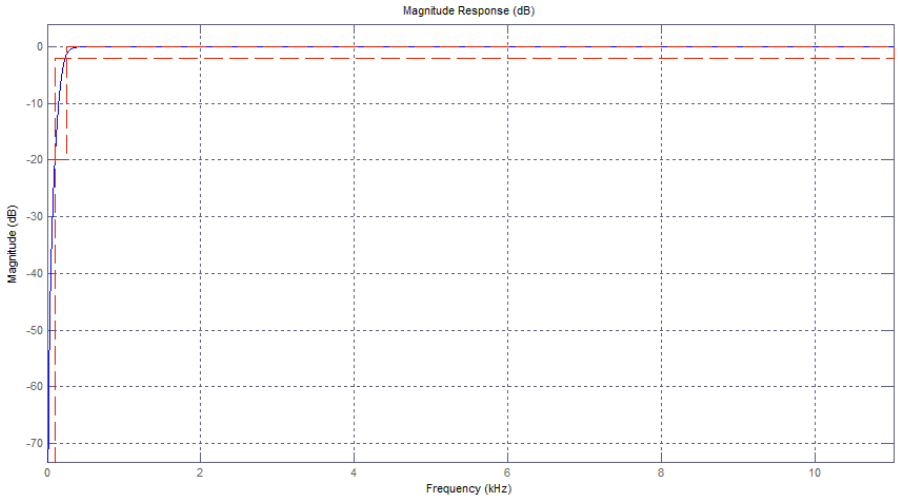


*Figure 63 – Highpass filter*

The filtered signal is shown in Figure 64.

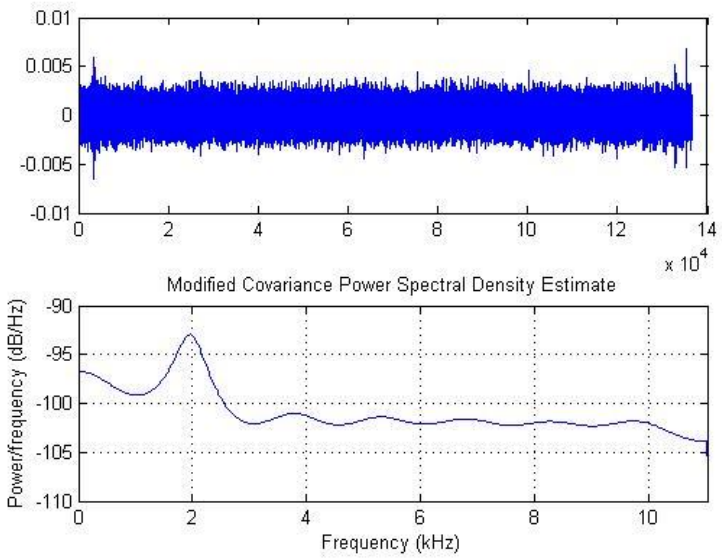


*Figure 64 - Spectrum after high pass filter*

The maximum value in this spectrum is the Doppler frequency for relevant velocity. A built in function in Matlab "max()" can return the maximum value in the spectrum. The equation of the velocity can be transformed from Equation (2.5).

$$f_d = \frac{2vcos\alpha}{c} f_0$$

The velocity is calculated as:

$$v = \frac{f_d c}{2 f_0 cos\alpha}$$

The results are shown in Table 4.

*Table 4 - Measured results*

| Velocity km/h | Estimated $f_d$ Hz | Measured $f_d$ Hz | Measured velocity km/h | Doppler frequency error |
|---|---|---|---|---|
| 20 | 629 | 602.9 | 19.1 | 4.1% |
| 30 | 943 | 775.2 | 24.7 | 17.8% |
| 40 | 1257 | 1055.1 | 33.6 | 16.1% |
| 60 | 1886 | 1636.5 | 52.1 | 13.3% |
| 70 | 2200 | 1959.5 | 62.4 | 11.0% |

The Doppler frequency error is calculated by the formula:

$$F_{d\_error} = \frac{|Estimated\ f_d - Measured\ f_d|}{Estimated\ f_d} \times 100\% \qquad (5.1)$$

The Doppler frequency deviation is largely between the estimated value and the practical measured value. The measured velocity is invalid. The error can be modified by changing the order in the AR methods. When the velocity is low, it needs a higher order for this method. Table 5 shows the modified values below:

*Table 5 - Modified results*

| Velocity km/h | Estimated $f_d$ Hz | Measured $f_d$ Hz | Modified measure velocity km/h | Minimum order | Doppler frequency error |
|---|---|---|---|---|---|
| 20 | 629 | 646.0 | 20.6 | 23 | 2.7% |
| 30 | 943 | 925.9 | 29.5 | 16 | 1.8% |
| 40 | 1257 | 1227.4 | 39.1 | 13 | 2.4% |
| 60 | 1886 | 1916.5 | 61.0 | 9 | 1.6% |
| 70 | 2200 | 2174.9 | 69.2 | 9 | 1.1% |

The results after modification by adjusting the order in the calculations are reasonable. When the vehicle moves slowly, the Doppler signal is weak. In this case, the order of the calculations should be higher. When the vehicle speeds up, the relative movement is much more obvious, and the Doppler signal is stronger. Therefore, the order should be a little lower.

The various order values add complexity. To get a real-time velocity of the moving vehicle, there should be a program to control the order value used in the computations. For example, the default value can be set as 23, and when the velocity reaches 20 km/h, the order value can be regulated down by 1 gradually.

# 6. Conclusion and outlook

## 6.1 Conclusion

This study stated a realization of measuring the velocity of vehicle with a Doppler radar. It follows the process step by step.

1. The Doppler Effect and the principle of the Doppler radar are introduced. The relation between the Doppler frequency and the velocity is deduced: $f_d = \frac{2v\cos\alpha}{c} f_0$.. This is the theoretical foundation of this thesis. Some other journal articles are referenced to introduce the applications of Doppler radar in other fields. The frequently used algorithms for spectrum estimation, such as the periodogram method, the Bartlett method, the Welch method, the BT method and the parametric methods are introduced.
2. A geometric model was built to simulate and estimate the Doppler signal. From this geometric model, the theoretical Doppler signal equation is found: $x(t) = \sum_{n=1}^{Grid\_no} \sqrt{P_r}_n e^{i(2\pi f_{d_n} + \theta)}$. The theoretical Doppler PSD is estimated and the result is illustrated in Figure 17. The maximum reflected power is -50 dBm when the radar is mounted on the vehicle 2 m above the ground.
3. A number of simulations showed the differences between these algorithms. The Welch method gives the best performance among the classical methods, but compared with the AR model, the resolution of the spectrum is not as good as the AR model. As a result, it was decided that the AR model algorithm should be implemented in this system.
4. The measured data were analyzed in Matlab and the spectra were shown. The results illustrate that:
    a. The real measured power spectrum is about -93 dBm, not as it was calculated theoretically as -50 dBm theoretically.
    b. This Doppler radar module should be fixed as low as possible to receive a better Doppler signal. The recommended place on the vehicle is on the vehicle chassis.
5. The peak values in the spectrum show that the Doppler frequency error is relatively large. To adjust the deviations, a program should be designed to control the order in calculations dynamically. The default order value is set equal to 23 and then decreases by one when the velocity reaches 20 km/h. The minimum order is 9 when the velocity is 70 km/h.

## 6.2 Outlook

This thesis illustrated a thought about how to utilize a Doppler radar to measure the velocity of vehicles. It displayed some achievements, but due to the time limitation, there are still drawbacks in our system.

1. This thesis only compared some often-used PSD algorithms, and picked out one of the best algorithms for our system. There are many PSD methods. The method implemented here may not be the best one.
2. There are some limitations in this thesis. The measurements were implemented on a sunny day, and the road surface was dry. We knew that the radar cross-section (RCS) differed according to whether the reflecting surface was dry, icy or wet. Our first limitation is that the reflecting surface should be dry. The second limitation is that the height of the radar should be set at no more than 0.5 m. Additionally, the third limitation is that there were some simplified calculations during the modeling process, and this may lead to some deviations.
3. This thesis focuses mainly on the theoretical analysis and discussion. There is still a long process to test, improve and complete this system. The selection of electronics elements, design of the circuits and filtering of the signal should be reconsidered to obtain a more precise, stable and quick-response Doppler radar speed measurement system.
4. Due to the time limitation, there is only one group of measurements. It is uncertain whether the errors shown in the results are caused by the algorithm or by some misoperations during the measurements; for example, the radar may shake when the vehicle is moving. More measurements should be taken to avoid the errors caused by misoperations.

# 7. References

[1] TutorVista. (2010). *Doppler Shift Formula*, Retrieved May 2013, from http://formulas.tutorvista.com/physics/doppler-shift-formula.html

[2] Kleinhempel, W., Bergmann, D., & Stammler, W. (1992). Speed measure of vehicles with on-board Doppler radar. *Radar 92. International Conference*, 284-287.

[3] Doviak, R. J., Zrnic, D. S., & Sirmans, D. S. (1979). Doppler weather radar. *Proceedings of the IEEE*, 67 (11), 1522-1553.

[4] John Wiley and Sons. (1991). *Range-Doppler.* Retrieved May 2013, from https://earth.esa.int/handbooks/asar/CNTR2-6-1-2-3.htm.

[5] Thornton, C. L. & Border, J. S. (2000). Chapter 3: Range and Doppler tracking observables. In J. H. Yuen (Ed.), *Deep Space Communications and Navigation Series* (pp. 9-46). California: Jet Propulsion Laboratory.

[6] Deming, R., Schindler, J., & Perlovsky, L. (2009). Multitarget/Multisensor Tracking using only Range and Doppler Measurements. *IEEE Transactions on Aerospace and Electronic Systems,* 45 (2), 593-611.

[7] Shapiro, I. I. Lincoln Laboratory, M.I.T. (1968). Planetary radar astronomy. *Spectrum, IEEE*, 5 (3), 70-79.

[8] Millis, J. P. (2012). *What is the Doppler Effect?* Retrieved May 2013, from http://www.library.usyd.edu.au/elearning/learn/referencing/index.php.

[9] Microwave Solutions Ltd. (2012). Instruction manual: Using Microwave Solutions Ltd Motion Detector Units-Application notes.

[10] Proakis, J. G. & Manolakis, D. G. (2007). 14.1.2: Estimation of the autocorrelation and power spectrum of random signals: The periodogram. In M. McDonald, A. Dworkin, V. O'Brien, D. A. George, & W. Kopf (Eds.), *Digital Signal Processing Principles, Algorithms and Applications* (4th ed., pp. 966-971). New Jersey: Pearson Education, Upper Saddle River.

[11] Proakis, J. G. & Manolakis, D. G. (2007). 14.2.1: The Bartlett Method: Averaging periodograms. In M. McDonald, A. Dworkin, V. O'Brien, D. A. George, & W. Kopf (Eds.), *Digital Signal Processing Principles, Algorithms and Applications* (4th ed. pp. 974-975). New Jersey: Pearson Education, Upper Saddle River.

[12] Proakis, J. G. & Manolakis, D. G. (2007). 14.2.2: The Welch Method: Averaging modified periodograms. In M. McDonald, A. Dworkin, V. O'Brien, D. A. George, & W. Kopf (Eds.), *Digital Signal Processing Principles, Algorithms and Applications* (4th ed. pp. 975-977). New Jersey: Pearson Education, Upper Saddle River.

[13] Proakis, J. G. & Manolakis, D. G. (2007). 14.2.3: The Blackman and Tukey Method: Smoothing the periodograms. In M. McDonald, A. Dworkin, V. O'Brien, D.

A. George, & W. Kopf (Eds.), *Digital Signal Processing Principles, Algorithms and Applications* (4th ed. pp. 978-981). New Jersey: Pearson Education, Upper Saddle River.

[14] Proakis, J. G. & Manolakis, D. G. (2007). 14.2.4: Performance characteristics of nonparametric power spectrum estimators. In M. McDonald, A. Dworkin, V. O'Brien, D. A. George, & W. Kopf (Eds.), *Digital Signal Processing Principles, Algorithms and Applications* (4th ed. pp. 981-984). New Jersey: Pearson Education, Upper Saddle River.

[15] Proakis, J. G. & Manolakis, D. G. (2007). 10.2.2: Design of linear-phase FIR filters using Windows. In M. McDonald, A. Dworkin, V. O'Brien, D. A. George, & W. Kopf (Eds.), *Digital Signal Processing Principles, Algorithms and Applications* (4th ed. pp. 664-670). New Jersey: Pearson Education, Upper Saddle River.

[16] Wikipedia. (2013). Window functions. Retrieved May 5, 2013, from http://en.wikipedia.org/wiki/Window_function.

[17] Proakis, J. G. & Manolakis, D. G. (2007). 14.3: Parametric methods for power spectrum estimation. In M. McDonald, A. Dworkin, V. O'Brien, D. A. George, & W. Kopf (Eds.), *Digital Signal Processing Principles, Algorithms and Applications* (4th ed. pp. 985-987). New Jersey: Pearson Education, Upper Saddle River.

[18] Proakis, J. G. & Manolakis, D. G. (2007). 3: The Z-Transform and its application to the analysis of LTI system. In M. McDonald, A. Dworkin, V. O'Brien, D. A. George, & W. Kopf (Eds.), *Digital Signal Processing Principles, Algorithms and Applications* (4th ed. pp. 985-987). New Jersey: Pearson Education, Upper Saddle River.

[19] Proakis, J. G. & Manolakis, D. G. (2007). 12.2.2: Relationships between the filter parameters and the autocorrelation sequence. In M. McDonald, A. Dworkin, V. O'Brien, D. A. George, & W. Kopf (Eds.), *Digital Signal Processing Principles, Algorithms and Applications* (4th ed. pp. 837-838). New Jersey: Pearson Education, Upper Saddle River.

[20] Proakis, J. G. & Manolakis, D. G. (2007). 12.4.1: The Levinson-Durbin algorithm. In M. McDonald, A. Dworkin, V. O'Brien, D. A. George, & W. Kopf (Eds.), *Digital Signal Processing Principles, Algorithms and Applications* (4th ed. pp. 847-850). New Jersey: Pearson Education, Upper Saddle River.

[21] Yu, R. & Lin, X. (2002). A multi-stage Levinson-Durbin algorithm. *Conference Record of the Thirty-Sixth Asilomar Conference on Signals, Systems and Computers, 2002* (Vol. 1), 218-221.

[22] Campbell, W. & Swingler, D. N. (1993). Frequency estimation performance of several weighted Burg algorithms. *Signal Processing, IEEE Transactions on,* 41 (3), 1237-1247.

[23] Proakis, J. G. & Manolakis, D. G. (2007). 14.3.3: The Burg Method for the AR model parameters. In M. McDonald, A. Dworkin, V. O'Brien, D. A. George, & W. Kopf (Eds.), *Digital Signal Processing Principles, Algorithms and Applications* (4th ed. pp. 991-994). New Jersey: Pearson Education, Upper Saddle River.

[24] Marple, L. (1980). A new autoregressive spectrum analysis algorithm. *Acoustics, Speech and Signal Processing, IEEE Transactions on,* 28 (4), 441-454.

[25] Microwave Solutions Ltd. (2012). Product data sheet: K-Band Doppler Motion Detector Units-Model Numbers MDU 2400/2410.

[26] Dybdal, R. B. (1987). Radar cross section measurement. *Proceedings of the IEEE,* 75 (4), 498-516.

[27] Viikari, V., Varpula, T., & Kantanen, M. (2008). Automotive radar technology for detecting road conditions. Backscattering properties of dry, wet, and icy asphalt. *Proceedings of the Radar Conference, 2008. EuRAD 2008. European.* 276-279.

[28] National Instruments. (2011). *Windowing: Optimizing FFTs Using Window Functions*. Retrieved May 5, 2013, from http://www.ni.com/white-paper/4844/en.

[29] Wikipedia. (2013). WAV. Retrieved May 5, 2013 from http://en.wikipedia.org/wiki/WAV#cite_note-MPI1-3.